

Breaking the Dimensional Barrier: Dynamic Portfolio Choice with Parameter Uncertainty via Pontryagin Projection

Jeonggyu Huh¹ and Hyeng Keun Koo²

¹Department of Mathematics, Sungkyunkwan University, Suwon, Republic of Korea
²Department of Financial Engineering, Ajou University, Suwon, Republic of Korea

January 16, 2026

Abstract

We study continuous-time CRRA portfolio choice in diffusion markets with uncertain estimated coefficients. Nature draws a latent parameter from a given distribution and keeps it fixed; the investor cannot observe this parameter and must commit to a parameter-blind policy maximizing an ex-ante objective. We treat the uncertainty distribution as an inference-agnostic sampling input.

We develop a simulation-only two-stage solver. Stage 1 extends Pontryagin-Guided Direct Policy Optimization (PG-DPO) by sampling parameters internally and computing gradients via backpropagation through time. Stage 2 performs an aggregated Pontryagin projection: it aggregates costates across the parameter distribution to enforce a deployable stationarity condition, yielding a structured correction amortized via interactive distillation.

We prove a uniform conditional BPTT-PMP correspondence and a residual-based policy-gap bound with explicit error terms. Experiments on high-dimensional Gaussian drift and factor-driven benchmarks show that projection stabilizes learning and accurately recovers analytic references, while a model-free PPO baseline remains far from the targets.

Keywords: Portfolio choice; Parameter uncertainty; Deep learning; Pontryagin principle; Stochastic control

1 Introduction

A central problem in quantitative finance is to allocate wealth dynamically across many risky assets in continuous time. In the classical Merton model, investment opportunities are described by a low-dimensional diffusion with *known* drift and volatility, and closed-form optimal portfolios follow from HJB analysis; see, for example, Merton (1969, 1971). In realistic markets, however, key inputs—especially expected returns—must be estimated from finite samples, often in high dimensions and under regularization/model selection. Empirically, return predictability is unstable and many predictors deliver limited out-of-sample gains (e.g., Goyal and Welch, 2008; Campbell and Thompson, 2008). These considerations motivate separating diffusion risk (Brownian noise conditional on parameters) from *decision-time estimation error* (uncertainty in estimated coefficients), a theme that also underlies intertemporal hedging and more conservative allocations in models with predictability/learning (e.g., Kandel and Stambaugh, 1996; Barberis, 2000; Campbell and Viceira, 2002; Xia, 2001; Maenhout, 2004).

We study continuous-time portfolio choice when market dynamics are known only up to an *estimated* parameter $\theta \in \Theta$, and an external estimation pipeline produces a nondegenerate

uncertainty law $q(d\theta)$ over Θ . We treat q as an *input* object that summarizes decision-time estimation error about θ . Concretely, q may be obtained from resampling-based approximations (e.g., the bootstrap) (e.g., Efron, 1979; Efron and Tibshirani, 1994), from subsample aggregation and model-selection variability (e.g., bagging), or from asymptotic (sandwich/normal) approximations of an estimator’s sampling distribution (van der Vaart, 1998). Our goal is not to revisit inference, but to optimize decisions *given* this uncertainty description. Algorithmically, we interact with q only through sampling $\theta \sim q$ inside a simulator; we do not assume a closed-form density, conjugacy, or a particular parametric family. We seek portfolio policies that maximize terminal CRRA utility *ex-ante*, averaging over both diffusion noise and parameter draws $\theta \sim q$.

A key modeling choice is that θ is *latent*: Nature draws a fixed but unobserved $\theta \sim q$ at time 0 (independent of the Brownian drivers) and keeps it fixed on $[0, T]$. The investor knows q but does not observe the realized θ and must therefore deploy a single θ -*blind* policy. We restrict attention to Markov feedback policies of the form $\pi_t = \bar{\pi}(t, X_t, Y_t)$ that depend only on observable wealth X_t and market factors Y_t , and we do *not* augment the state by a filtering/belief process. This is a one-shot *decision-time* problem: q is treated as fixed over the trading horizon, and we do not model or hedge subsequent updates of the uncertainty description. Belief-state control (optimal learning/hedging of parameter uncertainty) is conceptually important, but it defines a different and typically far more demanding problem than computing a single deployable θ -blind rule from a fixed q (e.g., Bensoussan and van Schuppen, 1985; Pham and Wei, 2017).

The θ -blind deployability constraint also changes what a first-order optimality condition means. Under full information, Pontryagin’s Maximum Principle (PMP) yields a θ -conditional criticality condition, hence a θ -conditional feedback map that is infeasible when θ is latent. Under θ -blind deployability, admissible perturbations are also θ -blind, and the correct necessary condition is q -*aggregated*: the expectation over $\theta \sim q$ of the Hamiltonian gradient $\partial_\pi H_\theta^{\text{ctrl}}$ must vanish along the controlled state process (e.g., Yong and Zhou, 1999; Fleming and Soner, 2006; Pham, 2009). In our portfolio setting, $\partial_\pi H_\theta^{\text{ctrl}}$ is affine in π , so q -aggregation yields a statewise linear system whose solution defines a deployable θ -blind *projection* map. This condition is inference-agnostic: it depends on q only through its role as the ex-ante mixing law.

These features place the problem beyond the reach of classical dynamic programming in the targeted high-dimensional regime. Even in moderate dimensions, HJB solvers face the curse of dimensionality (e.g., Bellman, 1961; Kushner and Dupuis, 2001). Although deep PDE (e.g., Raissi et al., 2019; Sirignano and Spiliopoulos, 2018) and BSDE methods (e.g., Han et al., 2018; Beck et al., 2019) reduce grid reliance, nonlinear portfolio HJBs remain numerically delicate. Furthermore, belief augmentation renders the problem infinite-dimensional (e.g., Bensoussan and van Schuppen, 1985; Pham and Wei, 2017). Accordingly, we exclude value-function solvers as practical baselines under our θ -blind interface, validating instead on closed-form benchmarks and simulation-only model-free RL (e.g., PPO).

Our approach is simulation-based and builds on *Pontryagin-Guided Direct Policy Optimization* (PG-DPO) (Huh et al., 2025a,b). PG-DPO parameterizes a θ -blind feedback policy via a neural network, simulates trajectories of the controlled SDE, and uses backpropagation through time (BPTT) to compute exact discrete-time gradients of terminal utility. Pathwise sensitivities computed by BPTT coincide with stochastic costates in PMP, reflecting the classical adjoint/backpropagation correspondence (e.g., LeCun, 1988; Yong and Zhou, 1999). In the latent-parameter setting, we sample $\theta \sim q$ *inside* the simulator (fixing it along each trajectory), while the policy depends only on observable states. To stabilize learning under heterogeneous θ draws, we develop uncertainty-aware *projected* P–PGDPO: after a warm-up phase that stabilizes costate estimates, we project Monte Carlo Pontryagin objects onto the q -aggregated PMP first-order condition, producing a robust deployable θ -blind rule that can be amortized into a fast policy.

Empirically, in high-dimensional static drift experiments, the projected pipeline improves

decision-time accuracy over end-to-end learning, stabilizing aligned regimes. In factor-driven markets where correlation induces hedging demand, it recovers analytic references under the θ -blind restriction, whereas a PPO baseline remains far off. Theoretically, we establish a residual-based policy-gap bound: under mild stability, a small aggregated residual implies the policy is close to a locally optimal deployable rule, up to discretization and Monte Carlo errors.

Our contributions are threefold. (i) We formulate a latent-parameter, fixed- q ex-ante CRRA portfolio problem under a deployable θ -blind Markov feedback restriction and derive the corresponding q -aggregated PMP first-order condition, emphasizing an inference-agnostic interface where uncertainty enters only through an exogenous mixing law $q(d\theta)$. (ii) We extend PG-DPO to this setting by sampling θ only inside the simulator and using BPTT to compute exact discrete-time gradients and pathwise sensitivities, and we establish a conditional BPTT-PMP correspondence uniform over θ on compact subsets of Θ . (iii) We develop uncertainty-aware P-PGDPO that projects Monte Carlo costate estimates to produce a deployable q -aggregated θ -blind rule, together with a residual-based ex-ante θ -blind policy-gap bound and empirical evidence of two-time-scale stabilization.

The remainder of the paper is organized as follows. Section 2 formulates the fixed- q ex-ante problem and derives θ -conditional versus q -aggregated PMP conditions together with Gaussian decision-time reference models. Section 3 develops PG-DPO and P-PGDPO for latent θ and proves the policy-gap bound. Sections 4 and 5 report numerical experiments, and the appendix collects technical proofs and implementation details.

2 Dynamic Portfolio Choice in Estimated Diffusion Markets with Latent Parameter Uncertainty

In this section we formalize a continuous-time CRRA portfolio problem in an estimated diffusion market with latent parameter uncertainty. Rather than fixing an inference architecture, we take as input an exogenous decision-time law $q(d\theta)$ over Θ and work with a latent, time-constant parameter $\theta \sim q$ (see Section 2.1 for the full model and objective). We adopt a θ -blind commitment viewpoint: the investor commits at the decision time to a single Markov feedback rule $\pi_t = \bar{\pi}(t, X_t, Y_t)$ and does not update q during trading. This restriction shifts the relevant optimality notion from infeasible θ -conditional (full-information) conditions to a q -aggregated Pontryagin stationarity condition within the θ -blind admissible class (Section 2.2). Closed-form Gaussian decision-time reference models used for validation are collected in Section 2.3.

2.1 Model and ex-ante objective in estimated diffusion markets

We interpret time 0 as the *decision time* and study portfolio choice on a fixed horizon $[0, T]$. The uncertainty law $q(d\theta)$ is an exogenous input available at the decision time and is treated as fixed over $[0, T]$ (no online belief updates during trading).

Estimated diffusion market family (conditional on a latent parameter). Drift and volatility are not assumed known. Instead, we consider a general multi-asset, multi-factor diffusion family indexed by $\theta \in \Theta \subset \mathbb{R}^k$, where θ represents the (possibly high-dimensional) parameter produced by an estimation procedure. Conditional on θ , the d risky assets and an m -dimensional factor process Y_t evolve as

$$\frac{dS_t}{S_t} = r \mathbf{1} dt + b(Y_t, \theta) dt + \sigma(Y_t, \theta) dW_t, \quad S_0 \in (0, \infty)^d, \quad (1)$$

$$dY_t = a(Y_t, \theta) dt + \beta(Y_t, \theta) dW_t^Y, \quad Y_0 = y \in \mathbb{R}^m, \quad (2)$$

where W and W^Y are Brownian motions (possibly of different dimension) that may be instantaneously correlated. We write the instantaneous covariance and return-factor cross-covariance

as

$$\Sigma(y, \theta) := \sigma(y, \theta)\sigma(y, \theta)^\top, \quad \Sigma_{SY}(y, \theta) := \sigma(y, \theta)\rho\beta(y, \theta)^\top, \quad (3)$$

where ρ is defined by $d\langle W, W^Y \rangle_t = \rho dt$. Thus $\Sigma(y, \theta) \in \mathbb{R}^{d \times d}$ and $\Sigma_{SY}(y, \theta) \in \mathbb{R}^{d \times m}$.

Uncertainty law $q(d\theta)$ and information structure. We summarize the uncertainty of the parameter θ , estimated from finite samples, by a probability distribution

$$q(d\theta). \quad (4)$$

We treat q as inference-agnostic; it may represent resampling-based distributions (e.g., bootstrap (Efron, 1979; Efron and Tibshirani, 1994), bagging (Breiman, 1996)) or asymptotic approximations (van der Vaart, 1998). For our purposes, q is a fixed decision-time input describing plausible market parameters over $[0, T]$.

Remark 1 (Latent parameter, observability, and admissible controls). *We interpret θ as a latent (unobserved) market parameter: at the (shifted) decision time 0, Nature draws an \mathcal{F}_0 -measurable random variable $\theta \sim q$ (independent of the Brownian drivers) and keeps it fixed over $[0, T]$. The investor knows q but does not observe the realized θ , so deployable portfolio rules cannot take θ as an input.*

We consider the observable market filtration

$$\mathcal{F}_t^{\text{obs}} := \sigma\{(S_s, Y_s) : 0 \leq s \leq t\}, \quad 0 \leq t \leq T, \quad (5)$$

where $\sigma\{\cdot\}$ denotes the σ -field generated by the observed asset and factor paths (with the usual augmentation). Admissible portfolio processes are required to be progressively measurable with respect to $(\mathcal{F}_t^{\text{obs}})$.

Throughout the paper we restrict attention to the Markov feedback subclass

$$\mathcal{A}^{\text{fb}} := \left\{ \pi \in \mathcal{A}^{\text{obs}} : \exists \bar{\pi} : [0, T] \times (0, \infty) \times \mathbb{R}^m \rightarrow \mathbb{R}^d \text{ s.t. } \pi_t = \bar{\pi}(t, X_t, Y_t) \right\}, \quad (6)$$

where \mathcal{A}^{obs} is defined below. This restriction reflects a fixed- q commitment model: the investor forms q at the decision time and does not perform online filtering/belief-state updates during $[0, T]$.

Whenever we display θ -conditional (full-information) controls or sensitivity objects, they are computed under frozen- θ simulations and are used only for offline diagnostics; the deployed policy class and the learned policy remain θ -blind.

Wealth dynamics and admissibility (given θ). For any fixed θ , the corresponding wealth dynamics under a portfolio process $\pi_t(\omega) \in \mathbb{R}^d$ adapted to $\mathcal{F}_t^{\text{obs}}$ are

$$\frac{dX_t^\pi}{X_t^\pi} = \left(r + \pi_t^\top b(Y_t, \theta) \right) dt + \pi_t^\top \sigma(Y_t, \theta) dW_t, \quad (7)$$

and we denote by \mathcal{A}^{obs} the set of progressively measurable portfolio processes adapted to $(\mathcal{F}_t^{\text{obs}})$ for which (7) admits a (strictly) positive wealth solution. In the Markovian feedback case $\pi \in \mathcal{A}^{\text{fb}}$ one may think of $\pi_t = \bar{\pi}(t, X_t, Y_t)$.

Ex-ante objective under latent θ (and simulator viewpoint). The investor evaluates policies under an *ex-ante* objective that averages over both diffusion noise for fixed θ and the parametric uncertainty encoded by (4):

$$J(\pi) := \mathbb{E}_{\theta \sim q} \left[\mathbb{E}[U(X_T^\pi) \mid \theta] \right] = \int_{\Theta} \mathbb{E}[U(X_T^\pi) \mid \theta] q(d\theta). \quad (8)$$

The corresponding optimization problem (under our feedback restriction) is

$$\sup_{\pi \in \mathcal{A}^{\text{fb}}} J(\pi). \quad (9)$$

Whenever it exists, we denote by

$$\pi^{*,\text{blind}} \in \arg \max_{\pi \in \mathcal{A}^{\text{fb}}} J(\pi)$$

an optimal θ -blind feedback for the fixed- q commitment problem (9). For each fixed θ , we also write $\pi^{*,\theta}$ for the (infeasible) θ -conditional *full-information* optimal control that would be available if θ were observed.

The θ -blind constraint makes (9) strictly harder than solving a separate control problem for each fixed θ , since the latter yields a θ -indexed full-information family. Ex-ante averaging in (8) can also create gradient cancellation across heterogeneous parameter draws when one attempts to learn a single global policy end-to-end. While an $\mathcal{F}_t^{\text{obs}}$ -adapted policy could, in principle, filter θ online and solve a belief-state control problem (see, e.g., Bensoussan and van Schuppen (1985); Pham and Wei (2017)), we do *not* pursue that formulation here.

Approximating the outer expectation in (8) amounts to sampling $\theta \sim q$ *inside the simulator* (once per trajectory or once per update), running (1)–(2) under that frozen draw, and updating a θ -blind feedback policy to perform well *on average* over such draws. This is the setting targeted by the simulation-based PG-DPO and P-PGDPO methods developed in Section 3.

Decision-time commitment and (optional) plug-in replanning. Throughout, we treat $q(d\theta)$ as an exogenous *decision-time* input and keep it fixed over the trading horizon $[0, T]$: within a single run, we do not update q using newly observed returns or additional data, and we do not hedge against future changes of the uncertainty description. If the decision is revisited at a later calendar time $t_0 \in (0, T)$, we interpret this as starting a *new* decision-time problem on the remaining horizon with an externally supplied law q_{t_0} .

Such a law may coincide with a static input (Section 2.3.1), may arise as a *model-implied predictive* (prior) propagation of an initial uncertainty through factor dynamics without conditioning on new observations (Section 2.3.2), or may be produced by an external filtering/estimation routine that outputs a time-indexed uncertainty description (Appendix A). Our model and algorithms are conditional on whichever q is supplied at the decision time and always freeze that input over the ensuing horizon.

2.2 Pontryagin optimality under latent parameters: full-information vs. aggregated conditions

This subsection records the Hamiltonian structure underlying our projection step and clarifies what “Pontryagin first-order conditions” mean when the market parameter θ is latent and admissible controls are θ -blind. Throughout, $q(d\theta)$ denotes the *decision-time* input law (Section 2.1) and is treated as fixed over the trading horizon $[0, T]$. All expectations in this subsection are taken conditional on the decision-time information (suppressed in notation).

In particular, we distinguish between (i) *θ -conditional* (full-information) criticality conditions that would apply if θ were observable (and are therefore infeasible under latent θ), and (ii) *q -aggregated* criticality conditions that characterize stationarity *within the θ -blind admissible class* for the fixed- q ex-ante objective. Our discussion follows standard stochastic control/PMP arguments for diffusion control (e.g. Yong and Zhou, 1999; Fleming and Soner, 2006; Pham, 2009). We also comment on the relationship to partial-information (belief-state) PMP, but we do not develop that formulation here.

A θ -conditional (full-information) Hamiltonian and first-order condition (infeasible under latent θ). Fix $\theta \in \Theta$ and suppose, for the moment, that θ were observable to the controller. In Markovian settings with sufficient smoothness, the θ -conditional value function $V^{*,\theta}(t, x, y)$ satisfies an HJB equation whose *control Hamiltonian* (the part depending on π) can be written explicitly using (3). For clarity, we define the *control Hamiltonian map* as a function of generic “sensitivity” inputs $(\varphi_x, \varphi_{xx}, \varphi_{xy})$:

$$\mathcal{H}_\theta^{\text{ctrl}}(t, x, y, \pi; \varphi_x, \varphi_{xx}, \varphi_{xy}) := x \pi^\top b(y, \theta) \varphi_x + \frac{1}{2} x^2 \pi^\top \Sigma(y, \theta) \pi \varphi_{xx} + x \pi^\top \Sigma_{SY}(y, \theta) \varphi_{xy}, \quad (10)$$

where $\varphi_x, \varphi_{xx} \in \mathbb{R}$ and $\varphi_{xy} \in \mathbb{R}^m$. In the full-information HJB interpretation, we evaluate (10) at $(\varphi_x, \varphi_{xx}, \varphi_{xy}) = (V_x, V_{xx}, V_{xy})$. In the Pontryagin interpretation used below, the same affine map is evaluated at the corresponding θ -conditional adjoint/sensitivity objects (denoted $(p^\theta, p_x^\theta, p_y^\theta)$ along a trajectory); in smooth Markov regimes these objects coincide with the indicated value derivatives.

The pointwise first-order condition for an interior optimizer is therefore

$$\partial_\pi \mathcal{H}_\theta^{\text{ctrl}} = x V_x^{*,\theta} b(y, \theta) + x^2 V_{xx}^{*,\theta} \Sigma(y, \theta) \pi + x \Sigma_{SY}(y, \theta) V_{xy}^{*,\theta} = 0, \quad (11)$$

where $V_x^{*,\theta}, V_{xx}^{*,\theta}, V_{xy}^{*,\theta}$ are evaluated at (t, x, y) . Assuming $\Sigma(y, \theta)$ is invertible and $V_{xx}^{*,\theta} < 0$, this yields the closed-form θ -conditional full-information portfolio rule

$$\pi^{*,\theta}(t, x, y) = -\frac{1}{x V_{xx}^{*,\theta}(t, x, y)} \Sigma(y, \theta)^{-1} \left(V_x^{*,\theta}(t, x, y) b(y, \theta) + \Sigma_{SY}(y, \theta) V_{xy}^{*,\theta}(t, x, y) \right). \quad (12)$$

This θ -indexed rule is *not deployable* under latent parameters; we record it only as a full-information benchmark and diagnostic reference. In our setting, deployable policies never take the realized θ as an input; θ is accessed only through sampling inside the simulator when approximating q -expectations.

q -aggregated Pontryagin condition for the θ -blind ex-ante problem (Markov feedback). We now return to the actual setting: θ is latent, policies are θ -blind, and we restrict attention to the Markov feedback class \mathcal{A}^{fb} (Remark 1). Under this restriction we neither perform online filtering of θ nor replace q by a time-varying posterior distribution. Accordingly, the relevant Pontryagin condition is not the θ -conditional criticality (11) enforced pointwise in θ , but rather a necessary condition for optimality *within the θ -blind admissible class* for the fixed- q objective (8).

To see why ex-ante aggregation enters the first-order condition, take any θ -blind admissible perturbation $h = \{h_t\}_{t \in [0, T]}$ that is progressively measurable with respect to the observation filtration $(\mathcal{F}_t^{\text{obs}})$ and square-integrable, and define $\pi^\varepsilon := \pi + \varepsilon h$ for small ε . For each fixed θ , the stochastic maximum principle yields the first-variation identity

$$\frac{d}{d\varepsilon} J^\theta(\pi^\varepsilon) \Big|_{\varepsilon=0} = \mathbb{E} \left[\int_0^T \partial_\pi \mathcal{H}_\theta^{\text{ctrl}}(t, X_t, Y_t, \pi_t; p_t^\theta, p_{x,t}^\theta, p_{y,t}^\theta)^\top h_t dt \Big| \theta \right], \quad (13)$$

where $(p_t^\theta, p_{x,t}^\theta, p_{y,t}^\theta)$ denotes the θ -conditional Pontryagin sensitivity/adjoint objects associated with the *fixed* policy π in the frozen- θ market. (Equivalently, (13) evaluates the same affine map $\partial_\pi \mathcal{H}_\theta^{\text{ctrl}}$ defined by (10), with (V_x, V_{xx}, V_{xy}) replaced by the corresponding Pontryagin objects along the controlled trajectory.) Because both π and h are θ -blind, taking the outer expectation over $\theta \sim q$ and using Fubini’s theorem gives

$$\frac{d}{d\varepsilon} J(\pi^\varepsilon) \Big|_{\varepsilon=0} = \mathbb{E} \left[\int_0^T \mathbb{E}_{\theta \sim q} \left[\partial_\pi \mathcal{H}_\theta^{\text{ctrl}}(t, X_t, Y_t, \pi_t; p_t^\theta, p_{x,t}^\theta, p_{y,t}^\theta) \right]^\top h_t dt \right]. \quad (14)$$

Hence, for an interior θ -blind optimum $\pi^{\star, \text{blind}}$, the first variation must vanish for all such perturbations h , which implies the aggregated first-order condition

$$\mathbb{E}_{\theta \sim q} \left[\partial_{\pi} \mathcal{H}_{\theta}^{\text{ctrl}}(t, X_t, Y_t, \pi_t; p_t^{\theta}, p_{x,t}^{\theta}, p_{y,t}^{\theta}) \right] = 0, \quad \text{a.s. for a.e. } t \in [0, T]. \quad (15)$$

Equation (15) is the correct necessary condition for the ex-ante problem under the θ -blind constraint. In particular, it is generally distinct from imposing (11) for each θ separately, because θ -conditional criticality cannot be enforced by a single deployable θ -blind policy.

To operationalize (15) in the Markov feedback class, fix a feedback policy $\pi \in \mathcal{A}^{\text{fb}}$ and, for each frozen θ , consider the corresponding θ -conditional Pontryagin sensitivity objects $(p_t^{\theta}, p_{x,t}^{\theta}, p_{y,t}^{\theta})$ along the induced state process. In smooth Markov regimes these coincide with spatial derivatives of a decoupling field and, in particular, reduce to (V_x, V_{xx}, V_{xy}) in the full-information setting; in our algorithms we estimate them pathwise by automatic differentiation (see Section 3).

For the portfolio Hamiltonian (10), $\partial_{\pi} \mathcal{H}_{\theta}^{\text{ctrl}}$ is affine in π . This motivates defining the θ -conditional ‘‘projection inputs’’

$$A_t^{\theta}(t, x, y) := x p_{x,t}^{\theta}(t, x, y) \Sigma(y, \theta) \in \mathbb{R}^{d \times d}, \quad (16)$$

$$G_t^{\theta}(t, x, y) := p_t^{\theta}(t, x, y) b(y, \theta) + \Sigma_{SY}(y, \theta) p_{y,t}^{\theta}(t, x, y) \in \mathbb{R}^d, \quad (17)$$

and their q -aggregated counterparts

$$A_t(t, x, y) := \mathbb{E}_{\theta \sim q} [A_t^{\theta}(t, x, y)], \quad G_t(t, x, y) := \mathbb{E}_{\theta \sim q} [G_t^{\theta}(t, x, y)]. \quad (18)$$

These objects summarize how the latent parameter affects the first-order stationarity condition through the θ -conditional sensitivities.

Theorem 1 (q -aggregated first-order condition under latent θ (deployable θ -blind stationarity)). *Consider the fixed- q ex-ante objective (8) over the θ -blind Markov feedback class \mathcal{A}^{fb} . Assume standard smoothness/integrability conditions ensuring validity of first variations within \mathcal{A}^{fb} and existence of the associated θ -conditional Pontryagin objects. If $\pi^{\star, \text{blind}}$ is a locally optimal interior policy in \mathcal{A}^{fb} , then (15) holds. Moreover, in the portfolio setting (10), the aggregated stationarity is equivalent to the statewise linear system*

$$A_t(t, x, y) \pi^{\star, \text{blind}}(t, x, y) = -G_t(t, x, y), \quad (t, x, y) \in [0, T] \times (0, \infty) \times \mathbb{R}^m, \quad (19)$$

(where A_t, G_t are defined by (18) using the θ -conditional Pontryagin objects generated by $\pi^{\star, \text{blind}}$). Whenever $A_t(t, x, y)$ is invertible on the working domain, (19) is equivalently expressed as the projected feedback rule

$$\pi^{\text{agg}}(t, x, y) = -A_t(t, x, y)^{-1} G_t(t, x, y). \quad (20)$$

Proof sketch. The conditional first-variation identity (13) is standard for diffusion control under a fixed parameter θ (e.g. Yong and Zhou, 1999; Fleming and Soner, 2006; Pham, 2009). Taking the outer expectation over $\theta \sim q$ yields (14). Since h is an arbitrary θ -blind admissible perturbation, vanishing of the first variation at an interior optimum implies (15). For the quadratic portfolio Hamiltonian (10), substituting the explicit expression for $\partial_{\pi} \mathcal{H}_{\theta}^{\text{ctrl}}$ and introducing (16)–(18) yields the linear system (19) and the projected form (20) whenever A_t is invertible. \square

Note that π^{agg} is generally *not* equal to the naive average $\mathbb{E}_{\theta \sim q} [\pi^{\star, \theta}(t, x, y)]$ of θ -conditional full-information controls, reflecting the noncommutativity between averaging over θ and solving a first-order condition. In particular, even if one could compute $\pi^{\star, \theta}$ for each θ , averaging these infeasible oracles does not, in general, enforce the deployable q -aggregated stationarity (15).

Remark 2 (Relation to belief-state/learning formulations). *If one allows history-dependent policies that explicitly infer θ from observed returns, a principled partial-information formulation introduces a time-varying posterior/belief state $q_t(\cdot) = \mathbb{P}(\theta \in \cdot \mid \mathcal{F}_t^{\text{obs}})$. In such belief-state problems, the corresponding PMP/Hamiltonian criticality condition is expressed in terms of conditional expectations under q_t (or, equivalently, conditional on $\mathcal{F}_t^{\text{obs}}$); see, e.g., Haussmann (1987); Li and Tang (1995); Baghery and Øksendal (2007). We do not pursue that learning/belief-state route here. Our algorithms and theory target the fixed- q , q -aggregated projection (20) under the θ -blind Markov feedback restriction.*

2.3 Gaussian references at a fixed decision time

This subsection collects Gaussian benchmarks that yield closed-form *decision-time reference* allocations. Fix a decision time $t \in [0, T)$ and suppose an external procedure provides an \mathcal{F}_t -measurable input law q_t for the uncertain premium parameter/state. We treat q_t as a decision-time input (not a belief process updated within a run): it is held fixed over the remaining horizon $[t, T]$ and the resulting references are used only as validation targets and controlled diagnostics (not as characterizations of the unrestricted optimum). If the decision is revisited at a later time t' , the reference can be recomputed by resolving the decision-time problem with the new input $q_{t'}$ (plug-in replanning).

We present two decision-time references. Section 2.3.1 considers *static* drift uncertainty and provides the controlled benchmark used in the high-dimensional scaling/geometry experiments of Section 4. Section 2.3.2 considers a mean-reverting (OU) premium factor with Gaussian decision-time uncertainty for the current factor level, which induces a horizon-dependent effective Gaussian law for the time-averaged premium and yields a tractable reference used in the hedging-demand recovery study of Section 5. Appendix A gives a linear–Gaussian illustration of how an external filtering routine may produce a time-indexed input law q_t ; it is included only as an input mechanism (plug-in replanning), not as a belief-state control formulation.

2.3.1 Static Gaussian drift uncertainty

We start from a time-homogeneous Gaussian benchmark in which the (vector) risk premium is an unobserved *static* parameter. This “unknown mean” specification is a standard device for isolating estimation risk/parameter uncertainty in portfolio choice (e.g., Kandel and Stambaugh, 1996; Barberis, 2000; Pástor, 2000). Fix a decision time $t \in [0, T)$ and remaining horizon $\tau := T - t$. The agent chooses a θ -blind policy on $[t, T]$, and all decision-time uncertainty about the (time-constant) premium is summarized by an \mathcal{F}_t -measurable law $q_t(d\theta)$, which we do not update over $[t, T]$.

Market model (static latent drift). Let d risky assets satisfy, for $s \in [t, T]$,

$$\frac{dS_s}{S_s} = r \mathbf{1} ds + \theta ds + \Sigma^{1/2} dW_s, \quad S_t \in (0, \infty)^d, \quad (21)$$

where $\Sigma \in \mathbb{R}^{d \times d}$ is symmetric positive definite and $\theta \in \mathbb{R}^d$ is a latent constant excess-return vector. At decision time t , uncertainty about θ is represented by the input law

$$\theta \sim q_t(d\theta). \quad (22)$$

A θ -blind portfolio fraction process $\pi_s \in \mathbb{R}^d$ generates wealth on $[t, T]$:

$$\frac{dX_s^\pi}{X_s^\pi} = (r + \pi_s^\top \theta) ds + \pi_s^\top \Sigma^{1/2} dW_s, \quad X_t^\pi = x > 0. \quad (23)$$

We evaluate the (conditional) decision-time objective by mixing over q_t :

$$J_t(\pi) := \mathbb{E}_{\theta \sim q_t} \left[\mathbb{E}[U(X_T^\pi) \mid \theta, \mathcal{F}_t] \right]. \quad (24)$$

Under full information and CRRA utility $U(x) = x^{1-\gamma}/(1-\gamma)$ ($\gamma > 0, \gamma \neq 1$), the oracle Merton rule is $\pi^*(\theta) = \frac{1}{\gamma}\Sigma^{-1}\theta$ (Merton, 1969, 1971), which is infeasible here because θ is latent.

Analytic q_t -references via portfolios constant over $[t, T]$. To obtain transparent closed-form targets, we temporarily restrict attention to portfolio fractions that are constant in trading time s on $[t, T]$:

$$\pi_s \equiv \pi \in \mathbb{R}^d, \quad s \in [t, T]. \quad (25)$$

The superscript ‘‘const’’ used below refers to this constancy in s . The resulting reference may still depend on the decision time t through the input q_t and on the remaining horizon $\tau = T - t$. (Decision-time constant-portfolio targets of this kind are closely connected to myopic/plug-in benchmarks used in the parameter-uncertainty literature; see, e.g., Barberis (2000); Pástor (2000).)

CRRA ($\gamma > 1$): tilted optimality and Gaussian shrinkage. For $\gamma > 1$ and constant π , conditional on θ the terminal wealth is lognormal and

$$J_t(\pi) = \frac{x^{1-\gamma}}{1-\gamma} \exp \left\{ (1-\gamma)r\tau - \frac{1}{2}\gamma(1-\gamma)\tau \pi^\top \Sigma \pi \right\} M_{q_t}((1-\gamma)\tau\pi), \quad (26)$$

where $M_{q_t}(u) := \mathbb{E}_{\theta \sim q_t}[\exp(u^\top \theta)]$ is the moment generating function of q_t . Any interior optimizer $\pi_{q_t, \gamma}^{\text{const}}(t, \tau)$ satisfies the tilted first-order condition

$$\gamma \Sigma \pi_{q_t, \gamma}^{\text{const}}(t, \tau) = \nabla_u \log M_{q_t}(u) \Big|_{u=(1-\gamma)\tau \pi_{q_t, \gamma}^{\text{const}}(t, \tau)}. \quad (27)$$

If the decision-time input is Gaussian,

$$q_t = \mathcal{N}(m_t, P_t), \quad P_t \succeq 0, \quad (28)$$

then $\nabla_u \log M_{q_t}(u) = m_t + P_t u$ and the reference reduces to the linear system

$$(\gamma \Sigma - (1-\gamma)\tau P_t) \pi_{q_t, \gamma}^{\text{const}}(t, \tau) = m_t, \quad (29)$$

hence

$$\pi_{q_t, \gamma}^{\text{const}}(t, \tau) = (\gamma \Sigma - (1-\gamma)\tau P_t)^{-1} m_t. \quad (30)$$

For $\gamma > 1$, this takes the familiar shrinkage form

$$\pi_{q_t, \gamma}^{\text{const}}(t, \tau) = (\gamma \Sigma + (\gamma-1)\tau P_t)^{-1} m_t, \quad (\gamma > 1), \quad (31)$$

which makes explicit how decision-time uncertainty P_t dampens exposures as the remaining horizon grows (a qualitative effect widely emphasized in return-predictability/parameter-uncertainty studies; see, e.g., Barberis (2000); Pástor (2000); Kandel and Stambaugh (1996)).

2.3.2 Mean-reverting Gaussian premium and an induced horizon-dependent reference

We next replace the static premium by a mean-reverting Gaussian premium factor, a standard reduced-form device for return predictability and intertemporal hedging (Campbell and Viceira, 2002; Xia, 2001). Fix a decision time $t \in [0, T)$ and remaining horizon $\tau := T - t$. At time t we take as input a Gaussian law for the current factor level Y_t (rather than a point estimate), capturing decision-time statistical uncertainty (e.g., interval-type uncertainty quantification, resampling variability, or asymptotic approximations). Holding this input fixed over $[t, T]$, OU propagation and time-averaging induce a *horizon-dependent* effective premium law; when $\rho \neq 0$, return-factor shock correlation adds a further quadratic term relevant for hedging demand (Campbell and Viceira, 2002; Xia, 2001).

OU premium dynamics. Let $Y_s \in \mathbb{R}^m$ be a premium factor following

$$dY_s = K(\bar{y} - Y_s) ds + \Xi dW_s^Y, \quad K \in \mathbb{R}^{m \times m} \text{ Hurwitz and invertible}, \quad (32)$$

where $\bar{y} \in \mathbb{R}^m$ and $\Xi \in \mathbb{R}^{m \times m}$. Risky excess returns satisfy

$$dR_s := \frac{dS_s}{S_s} - r\mathbf{1} ds = BY_s ds + \Sigma^{1/2} dW_s, \quad (33)$$

with instantaneous correlation

$$d\langle W, W^Y \rangle_s = \rho ds, \quad \rho \in \mathbb{R}^{d \times m}. \quad (34)$$

Decision-time input law for the factor. At decision time t , we take as input an \mathcal{F}_t -measurable Gaussian law for the current factor level,

$$Y_t \sim q_t(dy) = \mathcal{N}(m_t, P_t), \quad P_t \succeq 0. \quad (35)$$

A common special case is *purely model-implied predictive propagation* from an initial uncertainty $Y_0 \sim \mathcal{N}(m_0, P_0)$ without conditioning on observations:

$$\begin{aligned} m_t &= \bar{y} + e^{-Kt}(m_0 - \bar{y}), \\ P_t &= e^{-Kt}P_0e^{-K^\top t} + \int_0^t e^{-K(t-s)}\Xi\Xi^\top e^{-K^\top(t-s)} ds, \end{aligned} \quad (36)$$

which is an OU transition (prior-predictive) law and should not be interpreted as an information update. (References for return predictability and OU-style investment-opportunity dynamics include Campbell and Viceira (2002); Xia (2001).)

Induced Gaussian law for the time-averaged premium over $[t, T]$. Define the remaining-horizon integrated factor and the associated horizon-averaged *effective* premium:

$$I_{t,T} := \int_t^T Y_s ds \in \mathbb{R}^m, \quad \bar{\theta}_{t,\tau} := \frac{1}{\tau} B I_{t,T} \in \mathbb{R}^d. \quad (37)$$

Let

$$A(\tau) := K^{-1}(I - e^{-K\tau}) \in \mathbb{R}^{m \times m}.$$

Under the linear-Gaussian OU model, $I_{t,T}$ is Gaussian under the input law (35):

$$I_{t,T} \sim \mathcal{N}(m_I(t, \tau), C_I(t, \tau)),$$

with

$$m_I(t, \tau) = \mathbb{E}[I_{t,T}] = \tau\bar{y} + A(\tau)(m_t - \bar{y}), \quad (38)$$

$$C_I(t, \tau) := \text{Cov}(I_{t,T}) = A(\tau)P_tA(\tau)^\top + \int_0^\tau A(u)\Xi\Xi^\top A(u)^\top du. \quad (39)$$

Consequently, the horizon-averaged effective premium is Gaussian,

$$\bar{\theta}_{t,\tau} \sim \mathcal{N}(m_{\bar{\theta}}(t, \tau), P_{\bar{\theta}}(t, \tau)), \quad m_{\bar{\theta}}(t, \tau) = \frac{1}{\tau}Bm_I(t, \tau), \quad P_{\bar{\theta}}(t, \tau) = \frac{1}{\tau^2}BC_I(t, \tau)B^\top. \quad (40)$$

The pair $(m_{\bar{\theta}}(t, \tau), P_{\bar{\theta}}(t, \tau))$ is the horizon-dependent effective Gaussian law that we use as a controlled analytic input.

Closed-form decision-time references under portfolios constant over $[t, T]$. As in Section 2.3.1, we define an analytic reference by restricting to portfolio fractions that are constant in trading time s over $[t, T]$, i.e. $\pi_s \equiv \pi \in \mathbb{R}^d$. The superscript “const” below refers to this constancy in s ; the resulting reference may still depend on the decision time t through (m_t, P_t) and on the remaining horizon τ through OU averaging.

CRRA ($\gamma > 1$). When $\rho \neq 0$, return shocks and factor shocks are contemporaneously correlated, producing an additional quadratic term in the constant-portfolio objective (hedging-demand channel; see, e.g., Campbell and Viceira (2002); Xia (2001)). Define the cross-covariance between $I_{t,T}$ and the return Brownian increment $W_T - W_t$:

$$C_{IW}(\tau) := \text{Cov}(I_{t,T}, W_T - W_t) = \int_0^\tau A(u) \Xi \rho^\top du \in \mathbb{R}^{m \times d}, \quad (41)$$

and the induced symmetric cross term

$$M_{\text{cross}}(\tau) := B C_{IW}(\tau) (\Sigma^{1/2})^\top + \Sigma^{1/2} C_{IW}(\tau)^\top B^\top \in \mathbb{R}^{d \times d}. \quad (42)$$

Then the Gaussian decision-time reference under constant portfolios is characterized by

$$\left(\gamma \tau \Sigma + (\gamma - 1) (B C_I(t, \tau) B^\top + M_{\text{cross}}(\tau)) \right) \pi_{q_t, \gamma}^{\text{const}}(t, \tau) = B m_I(t, \tau), \quad (\gamma > 1). \quad (43)$$

Equivalently,

$$\pi_{q_t, \gamma}^{\text{const}}(t, \tau) = \left(\gamma \tau \Sigma + (\gamma - 1) (B C_I(t, \tau) B^\top + M_{\text{cross}}(\tau)) \right)^{-1} B m_I(t, \tau).$$

When $\rho = 0$, we have $C_{IW}(\tau) = 0$ and $M_{\text{cross}}(\tau) = 0$, and the reference reduces to the independence-case shrinkage form obtained by plugging the effective Gaussian law (40) into the static Gaussian formula of Section 2.3.1:

$$\pi_{q_t, \gamma}^{\text{const}}(t, \tau) = (\gamma \Sigma + (\gamma - 1) \tau P_{\bar{\theta}}(t, \tau))^{-1} m_{\bar{\theta}}(t, \tau), \quad (\rho = 0, \gamma > 1).$$

3 Pontryagin–Guided Policy Optimization under Latent Parameter Uncertainty

We solve the fixed- q ex-ante portfolio problem of Section 2 under a latent, time-constant parameter $\theta \sim q$. The deployed controller is θ -blind: it depends only on observable states (t, X_t, Y_t) and never conditions on the realized θ . Uncertainty enters only through sampling θ inside the simulator.

Our solver has two components. **Stage 1 (PG–DPO)** performs stochastic gradient ascent on $J(\varphi) = \mathbb{E}[U(X_T^{\pi_\varphi, \theta})]$ by differentiating through an Euler simulator via BPTT. **Stage 2 (P–PGDPO)** aggregates the BPTT costate blocks across $\theta \sim q$ and enforces the q -aggregated Pontryagin first-order condition, yielding a deployable projected control.

Section 3.1 establishes the conditional BPTT–PMP correspondence and specifies the adjoint blocks needed for projection. Section 3.2 develops the q -aggregated projection and a residual-based policy-gap bound. Practical coupling mechanisms (residual-form projection and interactive distillation) are deferred to Appendix F.

3.1 PG–DPO as stochastic gradient ascent and a conditional BPTT–PMP correspondence

Setup and objectives (frozen θ , deployable θ -blind feedback). A latent parameter $\theta \in \Theta$ is sampled from a fixed law $q(d\theta)$ *inside the simulator* and kept frozen along each

simulated trajectory. A deployable portfolio policy is a θ -blind Markov feedback rule represented by a neural network

$$\pi_\varphi : [0, T] \times (0, \infty) \times \mathbb{R}^m \rightarrow \mathbb{R}^d, \quad (t, x, y) \mapsto \pi_\varphi(t, x, y), \quad \varphi \in \mathbb{R}^p, \quad (44)$$

which does *not* take θ as an input. Conditional on a fixed frozen θ , the controlled state $(X_t^{\pi, \theta}, Y_t^{\theta})_{t \in [0, T]}$ evolves as

$$\frac{dX_t^{\pi, \theta}}{X_t^{\pi, \theta}} = \left(r + \pi_t^\top b(Y_t^{\theta}, \theta) \right) dt + \pi_t^\top \sigma(Y_t^{\theta}, \theta) dW_t, \quad X_0 = x > 0, \quad (45)$$

$$dY_t^{\theta} = a(Y_t^{\theta}, \theta) dt + \beta(Y_t^{\theta}, \theta) dW_t^Y, \quad Y_0 = y \in \mathbb{R}^m, \quad (46)$$

where (W, W^Y) may be instantaneously correlated as in Section 2. For each fixed θ we evaluate π_φ by the conditional objective

$$J^\theta(\varphi) := \mathbb{E}[U(X_T^{\pi_\varphi, \theta}) \mid \theta], \quad (47)$$

where the expectation is over Brownian paths in (45)–(46). The fixed- q ex-ante objective is

$$J(\varphi) := \mathbb{E}_{\theta \sim q}[J^\theta(\varphi)] = \mathbb{E}[U(X_T^{\pi_\varphi, \theta})], \quad (48)$$

where the last expectation is joint over $\theta \sim q$ and (W, W^Y) . Thus $\sup_\varphi J(\varphi)$ is a stochastic optimization problem in which θ is sampled inside the simulator while the policy remains θ -blind.

Discretization, sampling over θ , and baseline PG–DPO update. We discretize the horizon using an Euler scheme. In training we may sample initial states $z_0^{(i)} = (t_0^{(i)}, x_0^{(i)}, y_0^{(i)})$ from a user-chosen distribution ν on $[0, T] \times (0, \infty) \times \mathbb{R}^m$. Given $t_0^{(i)}$, we discretize $[t_0^{(i)}, T]$ into N steps with step size

$$\Delta t^{(i)} := \frac{T - t_0^{(i)}}{N}, \quad t_k^{(i)} := t_0^{(i)} + k\Delta t^{(i)}, \quad k = 0, \dots, N.$$

For episode i , we denote the discrete state by $(X_k^{(i)}, Y_k^{(i)})_{k=0, \dots, N}$ and write $\theta^{(i)}$ for the frozen parameter used to generate that simulated environment. Given π_φ and Brownian increments, the mapping

$$(x^{(i)}, y^{(i)}, \theta^{(i)}, \{\Delta W_k^{(i)}, \Delta W_k^{Y, (i)}\}_{k=0}^{N-1}, \varphi) \mapsto U(X_N^{(i)})$$

is a finite computational graph; automatic differentiation thus computes exact *discrete-time* gradients $\nabla_\varphi U(X_N^{(i)})$ for the chosen discretization.

A typical PG–DPO update samples a mini-batch $\{z_0^{(i)}\}_{i=1}^M \sim \nu$, samples latent parameters either independently per episode ($\theta^{(i)} \sim q$) or shared within the batch (one $\theta \sim q$ reused across i), simulates Euler rollouts, and performs stochastic gradient ascent. Suppressing episode indices and writing θ for the frozen draw used in the rollout, the Euler recursion is

$$\begin{aligned} Y_{k+1} &= Y_k + a(Y_k, \theta)\Delta t + \beta(Y_k, \theta)\Delta W_k^Y, \\ X_{k+1} &= X_k + X_k \left(r + \pi_\varphi(t_k, X_k, Y_k)^\top b(Y_k, \theta) \right) \Delta t + X_k \pi_\varphi(t_k, X_k, Y_k)^\top \sigma(Y_k, \theta) \Delta W_k, \end{aligned}$$

starting from $(t_0, X_0, Y_0) = (t_0^{(i)}, x_0^{(i)}, y_0^{(i)})$. The episode reward is

$$J^{(i)}(\varphi) := U(X_N^{(i)}), \quad (49)$$

and BPTT computes $\nabla_\varphi J^{(i)}(\varphi)$. The policy parameters are then updated (e.g. by Adam) as

$$\varphi \leftarrow \varphi + \alpha \frac{1}{M} \sum_{i=1}^M \nabla_\varphi J^{(i)}(\varphi). \quad (50)$$

Under standard interchange conditions (dominated convergence / uniform integrability for the discretized simulator), this is an unbiased stochastic gradient for the *discretized* ex-ante objective; as $\Delta t \rightarrow 0$ it approximates the continuous-time objective.

BPTT adjoints and their interpretation: first adjoint and second-adjoint blocks. BPTT returns not only $\nabla_\varphi J^{(i)}(\varphi)$ but also adjoint variables with respect to intermediate state variables. For a single episode (suppressing i and θ in notation), define the pathwise wealth adjoint

$$p_k := \frac{\partial U(X_N)}{\partial X_k}, \quad k = 0, \dots, N, \quad (51)$$

which is the discrete-time analogue of the *wealth-component first adjoint*. For the Pontryagin projection in Section 3.2, we also require curvature-type objects. In smooth Markov regimes these correspond to (V_{xx}, V_{xy}) ; in the stochastic maximum principle they are naturally interpreted as *blocks of the second adjoint*. Accordingly, we track the following discrete-time blocks (computed by higher-order automatic differentiation):

$$p_{x,k} := \frac{\partial p_k}{\partial X_k} = \frac{\partial^2 U(X_N)}{\partial X_k^2}, \quad p_{y,k} := \frac{\partial p_k}{\partial Y_k} = \frac{\partial^2 U(X_N)}{\partial Y_k \partial X_k}, \quad k = 0, \dots, N. \quad (52)$$

(Here $p_{y,k} \in \mathbb{R}^m$ is the wealth-factor cross block.) These are the discrete-time objects that enter the affine-in-control Hamiltonian gradient and hence the projection step.

Pathwise vs. SMP-adapted adjoints. The quantities in (51)–(52) are *pathwise* (samplewise) derivatives on the simulated computation graph and, for $k < N$, they need not be adapted to time- t_k information (they can depend on future increments). To connect them to the stochastic maximum principle (which yields adapted adjoint processes and associated martingale terms), one performs the standard conditional L^2 projection onto the span of the driving increments on each step, yielding a discrete-time BSDE representation. *Concretely*, for a fixed frozen θ and the simulator filtration

$$G_{t_k}^\theta := \sigma(\theta, \{W_s, W_s^Y : 0 \leq s \leq t_k\}) \quad (\text{with the usual augmentation}),$$

we define the *adapted (projected) discrete adjoints*

$$p_k^{\Delta t, \theta} := \mathbb{E}[p_k | G_{t_k}^\theta], \quad p_{x,k}^{\Delta t, \theta} := \mathbb{E}[p_{x,k} | G_{t_k}^\theta], \quad p_{y,k}^{\Delta t, \theta} := \mathbb{E}[p_{y,k} | G_{t_k}^\theta].$$

Theorem 2 concerns the convergence of these adapted discrete objects (together with the associated one-step BSDE martingale coefficients) to the continuous-time Pontryagin adjoints.

Theorem 2 (BPTT–PMP correspondence (conditional on θ , including second-adjoint blocks; uniform on compacts)). *Fix $\theta \in \Theta$ and assume standard regularity conditions ensuring (i) well-posedness of the θ -conditional forward SDE (45)–(46) under the θ -blind policy π_φ , and (ii) well-posedness of the associated θ -conditional stochastic maximum principle, including the wealth-component first adjoint and the relevant blocks of the second adjoint needed for the portfolio Hamiltonian gradient. Let $(p_t^\theta, p_{x,t}^\theta, p_{y,t}^\theta)$ denote these continuous-time Pontryagin objects under π_φ . In smooth Markov regimes, they coincide (along the controlled state process) with (V_x, V_{xx}, V_{xy}) for the θ -conditional value function.*

Let $(p_k, p_{x,k}, p_{y,k})$ be the discrete pathwise quantities computed by BPTT for the Euler discretization with step Δt , as defined in (51)–(52). Let $(p_k^{\Delta t, \theta}, p_{x,k}^{\Delta t, \theta}, p_{y,k}^{\Delta t, \theta})$ be their adapted projections onto $G_{t_k}^\theta$ as defined above, and let the associated discrete-time BSDE martingale coefficients be defined via the one-step conditional L^2 projection on each step. Then, as $\Delta t \rightarrow 0$, the projected (adapted) BPTT-induced discrete adjoints converge to their continuous-time counterparts in an appropriate mean-square sense (along trajectories). Moreover, for any compact set $K \subset \Theta$, the constants in the convergence bounds can be chosen uniformly for all $\theta \in K$.

Proof. See Appendix C. \square

Across $\theta \sim q$, these Pontryagin objects form a θ -indexed family. Baseline PG–DPO trains against the ex–ante objective (48) by repeatedly sampling $\theta \sim q$ inside the simulator, while the deployable policy remains θ -blind.

3.2 Projected PG–DPO under latent θ : q -aggregated projection, diagnostics, and a residual-based policy-gap bound

Stage 2 is a *projection step*. Given a warm-up deployable θ -blind feedback policy $\pi^{\text{warm}} = \pi_{\varphi^{\text{warm}}}$ (from stage 1), we estimate θ -conditional Pontryagin adjoint objects under frozen $\theta \sim q$ by BPTT/Monte Carlo, aggregate them across θ , and construct a deployable θ -blind policy by projecting onto the q -aggregated stationarity condition derived in Section 2.2. Equivalently, Stage 2 can be viewed as a plug-in approximation of one application of the population projection map $T(\pi) := -A_\pi^{-1} G_\pi^{\text{mix}}$ (defined below) evaluated at $\pi = \pi^{\text{warm}}$ on the working domain. The key point is that the aggregated first-order condition is *affine* in the portfolio control; hence it induces a statewise linear system and, on a suitable working domain, a concrete projection map from (estimated) adjoint objects to a portfolio rule.

Throughout, the adjoint objects used in projection consist of the *wealth-component first adjoint* together with the *relevant blocks of the second adjoint* (cf. Section 3.1): in smooth Markov regimes these correspond to (V_x, V_{xx}, V_{xy}) evaluated along the controlled state.

Working domain and norms. Fix a measurable working state domain $D \subset [0, T] \times (0, \infty) \times \mathbb{R}^m$ (e.g. a training/evaluation band) and a reference measure μ on D (e.g. an empirical state distribution induced by rollouts). For $h : D \rightarrow \mathbb{R}^n$ we write

$$\|h\|_{L^2(\mu)} := \left(\int_D \|h(z)\|^2 \mu(dz) \right)^{1/2}, \quad z = (t, x, y),$$

and for θ -indexed families (used when tracking frozen- θ quantities in analysis/inspection),

$$\|f\|_{L^2(q \otimes \mu)} := \left(\int_{\Theta} \int_D \|f^\theta(z)\|^2 \mu(dz) q(d\theta) \right)^{1/2}. \quad (53)$$

Mixed-moment q -aggregation under a warm-up policy. By Theorem 1, any locally optimal interior *deployable* θ -blind policy $\pi^{*, \text{blind}}$ for the fixed- q ex–ante problem satisfies the q -aggregated stationarity condition (15). In the portfolio Hamiltonian (10), this stationarity is equivalent to a statewise linear system and hence to the projected form (20) on the working domain (under invertibility of the aggregated curvature term). P–PGDPO constructs a practical approximation of this projection by estimating the relevant aggregated Pontryagin objects under a fixed warm-up policy $\pi^{\text{warm}} = \pi_{\varphi^{\text{warm}}}$.

Fix a query state $z = (t, x, y) \in D$ and a frozen parameter θ . We simulate trajectories under π^{warm} and compute discrete-time adjoint blocks by autodiff/BPTT on the Euler simulator; averaging over M_{MC} trajectories yields Monte Carlo estimates

$$\hat{p}_t^\theta(z), \quad \hat{p}_{x,t}^\theta(z), \quad \hat{p}_{y,t}^\theta(z), \quad (54)$$

where \hat{p}_t^θ corresponds to the wealth-component first adjoint and $(\hat{p}_{x,t}^\theta, \hat{p}_{y,t}^\theta)$ correspond to the blocks of the second adjoint relevant for the Hamiltonian gradient. In the analysis, these are interpreted as estimators of the corresponding θ -conditional Pontryagin objects (cf. the conditional BPTT–PMP correspondence in Section 3.1).

Using these, define the θ -conditional estimated projection inputs

$$\hat{A}_t^\theta(t, x, y) := x \hat{p}_{x,t}^\theta(t, x, y) \Sigma(y, \theta) \in \mathbb{R}^{d \times d}, \quad (55)$$

$$\hat{G}_t^\theta(t, x, y) := \hat{p}_t^\theta(t, x, y) b(y, \theta) + \Sigma_{SY}(y, \theta) \hat{p}_{y,t}^\theta(t, x, y) \in \mathbb{R}^d, \quad (56)$$

where $\Sigma(\cdot, \theta)$ and $\Sigma_{SY}(\cdot, \theta)$ are the instantaneous covariance objects appearing in the θ -conditional Hamiltonian (as in Section 2).

Aggregating across $\theta \sim q$ (approximated in practice by sampling M_θ frozen parameters) gives the *mixed-moment* estimators

$$\hat{A}_t(t, x, y) := \mathbb{E}_{\theta \sim q} [\hat{A}_t^\theta(t, x, y)], \quad (57)$$

$$\hat{G}_t^{\text{mix}}(t, x, y) := \mathbb{E}_{\theta \sim q} [\hat{G}_t^\theta(t, x, y)]. \quad (58)$$

Whenever $\hat{A}_t(t, x, y)$ is invertible on D , we obtain the mixed-moment projected policy

$$\hat{\pi}^{\text{agg,mix}}(t, x, y) := -\hat{A}_t(t, x, y)^{-1} \hat{G}_t^{\text{mix}}(t, x, y). \quad (59)$$

Stabilized inversion and projection diagnostics (implementation). In practice, finite-sample estimates can make \hat{A}_t ill-conditioned or even singular on parts of D . Our default implementation therefore uses standard stabilizers (Appendix E.5), including: (i) ridge regularization $\hat{A}_{t,\lambda} := \hat{A}_t + \lambda I_d$ and $\hat{\pi}_\lambda^{\text{agg,mix}} := -\hat{A}_{t,\lambda}^{-1} \hat{G}_t^{\text{mix}}$, (ii) condition-number or eigenvalue diagnostics to skip/clip projection on unreliable states (falling back to π^{warm}), and (iii) residual-form projection (Section F.1) to reduce variance. The analysis below is stated for the population projection $T(\pi) := -A_\pi^{-1} G_\pi^{\text{mix}}$ and for small estimator perturbations, which is precisely the regime enforced by these stabilizers.

Remark (decoupled aggregation heuristic). The mixed-moment aggregation (57)–(58) is the object appearing in the exact q -aggregated first-order condition. In some high-dimensional experiments, we additionally consider a variance-reduction heuristic that replaces mixed moments by products of empirical means, e.g. $\mathbb{E}_\theta[\hat{p}_t^\theta b(y, \theta)] \approx \mathbb{E}_\theta[\hat{p}_t^\theta] \cdot \mathbb{E}_\theta[b(y, \theta)]$, and similarly for the other terms. All theoretical statements in this subsection are for the mixed-moment projection (59).

Residual diagnostic and a slab-wise small-gain policy-gap bound. To connect (59) to a locally optimal deployable θ -blind policy, we measure how well the warm-up policy satisfies the *population* mixed-moment aggregated stationarity. Let $(A_\pi, G_\pi^{\text{mix}})$ denote the mixed-moment q -aggregated projection inputs induced by a policy π (i.e. the objects in (18) evaluated using the θ -conditional Pontryagin adjoint blocks generated by π). Define the warm-up aggregated stationarity residual on D by

$$r_{\text{FOC,mix}}^{\text{warm}}(t, x, y) := A_{\pi^{\text{warm}}}(t, x, y) \pi^{\text{warm}}(t, x, y) + G_{\pi^{\text{warm}}}^{\text{mix}}(t, x, y), \quad \varepsilon_{\text{warm}}^{\text{mix}} := \|r_{\text{FOC,mix}}^{\text{warm}}\|_{L^2(\mu)}. \quad (60)$$

Note that $r_{\text{FOC,mix}}^{\text{warm}} = 0$ is equivalent to π^{warm} being a fixed point of T on D . More generally, the population projection admits the residual form

$$T(\pi^{\text{warm}}) = \pi^{\text{warm}} - A_{\pi^{\text{warm}}}^{-1} r_{\text{FOC,mix}}^{\text{warm}}. \quad (61)$$

In practice we monitor the empirical analogue $\hat{r}_{\text{FOC,mix}}^{\text{warm}} := \hat{A}_t \pi^{\text{warm}} + \hat{G}_t^{\text{mix}}$, and use it as a diagnostic to flag states where projection is unreliable (cf. Appendix E.5). (Equivalently,

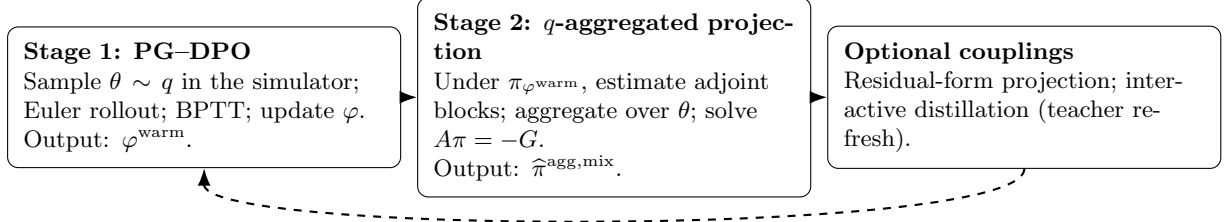


Figure 1: Two-stage pipeline of Section 3. A detailed schematic (including the coupling mechanisms and implementation notes) is provided in Appendix F, Fig. 4.

$\hat{\pi}^{\text{agg,mix}} = \pi^{\text{warm}} - \hat{A}_t^{-1} \hat{r}_{\text{FOC,mix}}^{\text{warm}}$, or its stabilized variant, which motivates the residual-form implementation.)

BPTT/Monte Carlo error term (one explicit choice). To make the discretization/Monte Carlo dependence in (65) explicit, one may take for example

$$\delta_{\text{BPTT}}(\Delta t, M_{\text{MC}}, M_{\theta}) := \|\hat{A}_t - A_{\pi^{\text{warm}}}\|_{L^2(\mu)} + \|\hat{G}_t^{\text{mix}} - G_{\pi^{\text{warm}}}^{\text{mix}}\|_{L^2(\mu)}. \quad (62)$$

Under standard Lipschitz/bounded-moment assumptions (Euler strong error and Monte Carlo sampling error), one typically has a scaling of the form $\delta_{\text{BPTT}}(\Delta t, M_{\text{MC}}, M_{\theta}) \lesssim \Delta t^{1/2} + M_{\text{MC}}^{-1/2} + M_{\theta}^{-1/2}$, up to constants depending on the working domain and stability bounds.

A technical point is that a *global* small-gain condition of the form $C_1 < 1$ can be overly restrictive. Following the slab-wise philosophy in our prior PGDPO analysis (e.g. Huh et al. (2025a, Appendix B)), we default to a *time-slab* decomposition of the working domain and close the warm-up gap on each short slab. Concretely, assume D carries a time coordinate and fix a partition $0 = t_0 < t_1 < \dots < t_K = T$ with slab lengths $\tau_k := t_k - t_{k-1}$. Let

$$D_k := D \cap ([t_{k-1}, t_k] \times \mathcal{S}), \quad \mu_k := \mu|_{D_k}, \quad \|f\|_k := \|f\|_{L^2(\mu_k)}.$$

We write $T(\pi) := -A_{\pi}^{-1} G_{\pi}^{\text{mix}}$ for the (population) q -aggregated projection map. Theorem 3 below shows that, under a mild *slab-wise* local stability regime (i.e. a short-time contraction of T on each D_k), small residual implies that the projected policy is close (in $L^2(\mu)$) to a locally optimal deployable θ -blind policy, up to discretization/Monte Carlo error. The proof combines a projection-map stability bound (Appendix D.1) with a slab-wise closure (Appendix D.2), in the same spirit as the slab analyses used in Huh et al. (2025a).

Theorem 3 (Residual-based ex-ante θ -blind policy-gap bound for P-PGDPO (mixed-moment, deployable, slab-wise local)). *Assume the uniform invertibility/stability conditions of Proposition 1 (Appendix D.1) hold on D for the relevant aggregated curvature terms and for the estimator perturbations constructed under π^{warm} (in particular, that \hat{A}_t remains a small perturbation of $A_{\pi^{\text{warm}}}$ on D under the adopted stabilizers).*

Let $\pi^{,\text{blind}}$ be a locally optimal interior deployable θ -blind policy for the fixed- q ex-ante problem. Assume there exists a neighborhood \mathcal{U} of $\pi^{*,\text{blind}}$ in $L^2(\mu)$ such that for all $\pi \in \mathcal{U}$,*

$$\|A_{\pi}^{-1}\|_{L^{\infty}(D)} \leq \kappa, \quad \|G_{\pi}^{\text{mix}}\|_{L^{\infty}(D)} \leq M_G,$$

and assume the slab-wise Lipschitz gain of Appendix D.2 holds: there exist constants $\bar{L}_A, \bar{L}_G > 0$ such that for every slab D_k and all $\pi_1, \pi_2 \in \mathcal{U}$,

$$\|A_{\pi_1} - A_{\pi_2}\|_k \leq \bar{L}_A \tau_k^{1/2} \|\pi_1 - \pi_2\|_k, \quad \|G_{\pi_1}^{\text{mix}} - G_{\pi_2}^{\text{mix}}\|_k \leq \bar{L}_G \tau_k^{1/2} \|\pi_1 - \pi_2\|_k. \quad (63)$$

Define

$$\rho(\tau) := (\kappa \bar{L}_G + \kappa^2 M_G \bar{L}_A) \tau^{1/2}, \quad \rho_* := \max_{1 \leq k \leq K} \rho(\tau_k). \quad (64)$$

Assume the slab partition is chosen so that $\rho_* < 1$.

Let $\hat{\pi}^{\text{agg,mix}}$ be the mixed-moment projected policy (59) computed from BPTT/Monte Carlo estimates under π^{warm} (with stabilized inversion as needed), and let $\varepsilon_{\text{warm}}^{\text{mix}}$ be the population residual (60). Then there exists $C_2 > 0$ such that

$$\|\hat{\pi}^{\text{agg,mix}} - \pi^{\star,\text{blind}}\|_{L^2(\mu)} \leq \frac{\rho_* \kappa}{1 - \rho_*} \varepsilon_{\text{warm}}^{\text{mix}} + C_2 \delta_{\text{BPTT}}(\Delta t, M_{\text{MC}}, M_{\theta}), \quad (65)$$

where one admissible explicit choice of δ_{BPTT} is given in (62). Moreover, under the perturbative regime of Proposition 1, one may take for example $C_2 := 2\kappa + 4\kappa^2 M_G$.

Proof. See Appendix D.3. □

Coupling and amortization. Figure 1 summarizes the overall two-stage design. Stage 2 is used purely as a warm-started *post-processing* map: it reuses the current stage 1 policy, estimates the adjoint blocks under frozen $\theta \sim q$, and outputs a single deployable θ -blind projected rule. For numerical stability and amortized deployment, we additionally consider (i) a residual/control-variate form of the projection and (ii) interactive distillation of the projected rule into the policy network. These practical coupling mechanisms are described in Appendix F.

4 Breaking the Dimensional Barrier under Drift Uncertainty

This section instantiates the decision-time *static* Gaussian drift-uncertainty benchmark from Section 2.3.1 and uses its closed-form constant-portfolio q -reference as an analytic target. Nature draws a latent drift $\theta \sim q$ at $t = 0$ and keeps it constant over $[0, T]$, while the investor cannot observe θ and must deploy a single θ -blind policy under an ex-ante CRRA objective. Because the benchmark admits a transparent decision-time reference, we can measure accuracy directly via a decision-time Euclidean RMSE to the analytic reference, rather than relying only on realized utility.

Our goal is to test whether Pontryagin-guided learning and projection remain stable as the number of assets grows. We generate APT-style covariance structures and sweep dimensions $d \in \{5, 10, 50, 100\}$ under both *aligned* uncertainty ($P = s\Sigma$) and a *misaligned* geometry that rotates uncertainty away from market risk directions. We compare Stage 1 (PG–DPO) to Stage 2 (Pontryagin projection), and (when applicable) amortized variants via interactive distillation, under Monte Carlo budgets that scale linearly with d .

4.1 Benchmark market and evaluation protocol

This subsection fixes the benchmark and evaluation protocol used in Section 4. Our goal is to provide controlled evidence that the proposed two-stage pipeline remains *computationally stable and accurate* as the number of assets d grows under *decision-time* parameter uncertainty. The aligned vs. misaligned uncertainty geometries serve as two representative stress-test regimes; the main message is scalability under uncertainty rather than any specific choice of P .

θ -blind deployability (and what uses θ). Throughout Section 4, *all reported policies are deployable and θ -blind*: the control is a function of observable state only (here, decision-time evaluation uses (t, X_0) with fixed horizon T), and *never takes the realized latent premium θ as an input*. The latent $\theta \sim q$ is sampled *only inside the simulator* to generate trajectories and to form Monte Carlo averages that approximate q -expectations (notably in Stage 2 projection). Any θ -indexed objects (when referenced elsewhere) are used only for *offline diagnostics* and are not part of the deployable decision rule.

Static decision-time uncertainty benchmark. We adopt the static Gaussian drift-uncertainty market of Section 2.3.1, i.e., (21) with (28). Equivalently, we simulate

$$\frac{dS_t}{S_t} = r \mathbf{1} dt + \theta dt + \Sigma^{1/2} dW_t, \quad \theta \sim \mathcal{N}(m, P),$$

where the latent premium θ is drawn once at time 0 and kept fixed over $[0, T]$. The deployable policy is θ -blind and interacts with q only through sampling θ inside the simulator.

APT-style factor construction of (m, Σ) . We construct the mean premium and covariance via a low-dimensional factor representation in the spirit of arbitrage pricing theory (APT) Ross (1976). Let W^f be a k_Σ -dimensional Brownian motion (factor shocks) and W^ε a d -dimensional Brownian motion (idiosyncratic shocks), independent of W^f . We write excess returns as

$$dR_t := \frac{dS_t}{S_t} - r \mathbf{1} dt = \theta dt + B \Sigma_f^{1/2} dW_t^f + \text{diag}(\sqrt{D}) dW_t^\varepsilon, \quad (66)$$

with $B \in \mathbb{R}^{d \times k_\Sigma}$, $\Sigma_f \succ 0$, and $D \in (0, \infty)^d$. This implies

$$\Sigma = B \Sigma_f B^\top + \text{diag}(D) = FF^\top + \text{diag}(D), \quad (67)$$

where $F := B \text{chol}(\Sigma_f)$. We generate the mean premium in an APT-like form by drawing a factor price vector $\lambda_m \in \mathbb{R}^{k_\Sigma}$ and setting

$$m := B \lambda_m. \quad (68)$$

One-shot generation and fairness across methods. For each dimension d , we generate a single market instance $(B, \Sigma_f, D, \lambda_m)$ once (using a fixed random seed) and *hold it fixed across all algorithmic comparisons and MC-budget variants*. Within a fixed d , we change only the uncertainty covariance P (aligned vs. misaligned and the scale s below). This isolates algorithmic effects from instance-to-instance randomness and makes the scaling comparisons controlled.

Uncertainty regimes (aligned vs. misaligned). We consider two geometries for the drift-uncertainty covariance P , controlled by a scalar magnitude $s > 0$.

Aligned: uncertainty shares market risk directions,

$$P = s \Sigma, \quad s > 0. \quad (69)$$

Misaligned: uncertainty factors are rotated away from the market factor space,

$$P = \tilde{B} \tilde{\Sigma}_f \tilde{B}^\top + s \text{diag}(D), \quad (70)$$

where \tilde{B} is generated independently of B (and can be orthogonalized against the span of B to enforce large principal angles). The factor term is rescaled to match the aligned factor magnitude under the same s ; concretely, writing $\Sigma_{\text{fac}} := B \Sigma_f B^\top$ and $\tilde{\Sigma}_{\text{fac}} := \tilde{B} \tilde{\Sigma}_f \tilde{B}^\top$, we rescale $\tilde{\Sigma}_{\text{fac}}$ so that $\text{tr}(\tilde{\Sigma}_{\text{fac}}) = \text{tr}(s \Sigma_{\text{fac}})$ while keeping the diagonal term fixed as $s \text{diag}(D)$. This geometry increases heterogeneity across $\theta \sim q$ and makes mixed-moment estimation and subsequent linear-algebra steps more fragile, providing a stringent scalability test.

Experiment grid and simulation budgets. We vary the number of assets over $d \in \{5, 10, 50, 100\}$ and sweep three uncertainty magnitudes $s \in \{10^{-3}, 10^{-2}, 10^{-1}\}$ for both aligned and misaligned geometries. To keep Monte Carlo noise comparable across dimensions, we use linear-in- d trajectory budgets: a *base* regime with $N_{\text{MC}} = 100 \cdot d$ rollouts and a *high* regime with $N_{\text{MC}} = 400 \cdot d$ rollouts. Here N_{MC} denotes the number of *independent simulated trajectories* used to approximate the relevant q -expectations (in Stage 1 for stochastic gradient estimates,

and in Stage 2 for costate/mixed-moment estimators at queried states). Each trajectory draws its own latent $\theta \sim q$ at time 0 and its own Brownian path thereafter; we do not use a separate inner loop of θ -samples per trajectory. All methods share the same discretization scheme (Euler) and the same market instances within each d ; implementation details (network architecture, optimizer settings, and exact sampling conventions for Stage 1 vs. Stage 2) are reported in the implementation appendix and code release.

Analytic reference and decision-time evaluation. In the static Gaussian benchmark, the analytic decision-time reference under constant portfolios is available in closed form. We use this closed-form rule only as an external decision-time target for evaluation; training does not impose the constant-portfolio restriction, and all methods learn from simulated trajectories over $[0, T]$ under the same θ -blind constraint. For $\gamma > 1$ we use the CRRA reference (31). We evaluate each method at $t = 0$ with a fixed horizon $T = 1.5$ on a fixed grid $\{X_0^{(i)}\}_{i=1}^{N_{\text{eval}}}$ and report Euclidean RMSE to the analytic reference:

$$\text{RMSE}(u_0, \pi_{q,\gamma}^{\text{const}}) := \left(\frac{1}{N_{\text{eval}}} \sum_{i=1}^{N_{\text{eval}}} \|u_0(X_0^{(i)}, T) - \pi_{q,\gamma}^{\text{const}}(T)\|^2 \right)^{1/2}, \quad (71)$$

where $\|\cdot\|$ is the Euclidean norm on \mathbb{R}^d and $u_0(\cdot)$ denotes the decision-time action prescribed by the method (deployable θ -blind output). With the benchmark fixed and with (m, Σ, P) constructed as in (68)–(70), the remaining subsections compare baseline Stage 1 PG–DPO, post-hoc Stage 2 P–PGDPO projection, and interactive distillation under matched simulation budgets.

4.2 High-dimensional CRRA benchmark: projection and amortization

Mixed-moment estimation and a decoupling approximation. A practical issue throughout our experiments (both aligned and misaligned) is the estimation of *mixed moments* across the latent parameter, such as $\mathbb{E}_{\theta \sim q}[p_t^\theta(z) \theta]$ (and analogous products entering \hat{G}_t^{mix}), because the costate $p_t^\theta(z)$ is θ -dependent and high-dimensional, and finite-sample covariance between p_t^θ and θ can lead to large Monte-Carlo variance once the subsequent linear solve is applied. For numerical stability and a uniform protocol across geometries, we therefore use a simple *decoupling* (independence) approximation for these mixed moments,

$$\mathbb{E}_{\theta \sim q}[p_t^\theta(z) \theta] \approx \mathbb{E}_{\theta \sim q}[p_t^\theta(z)] \mathbb{E}_{\theta \sim q}[\theta],$$

(and similarly for other mixed products), which is exact when the relevant Pontryagin objects are effectively θ -invariant and is accurate whenever $\text{Cov}_q(p_t^\theta(z), \theta)$ is small relative to marginal scales. While this approximation is most valuable under misalignment—where direction mixing can amplify mixed-moment noise—it also performs well in aligned regimes (where mixed moments are typically easier to estimate), and in the CRRA benchmark below it does not alter the qualitative scaling conclusions: projection remains stable, and the observed misaligned degradation is consistent with residual growth and curvature mismatch rather than catastrophic mixed-moment blow-ups.¹

Protocol and summary statistic. We consider the CRRA benchmark with $\gamma = 2$ under Gaussian drift uncertainty q and evaluate against the analytic constant q -reference (31). We track (i) the Monte-Carlo objective estimate \hat{J} during training and (ii) the decision-time error at $t = 0$ via RMSE (71) with fixed horizon $T = 1.5$. Because stochastic optimization produces

¹We note, however, that in extreme uncertainty/misalignment—where θ -costate dependence becomes pronounced—the decoupling can break down, in which case one should revert to full mixed-moment estimation (possibly with larger budgets and/or regularized/certified projection).

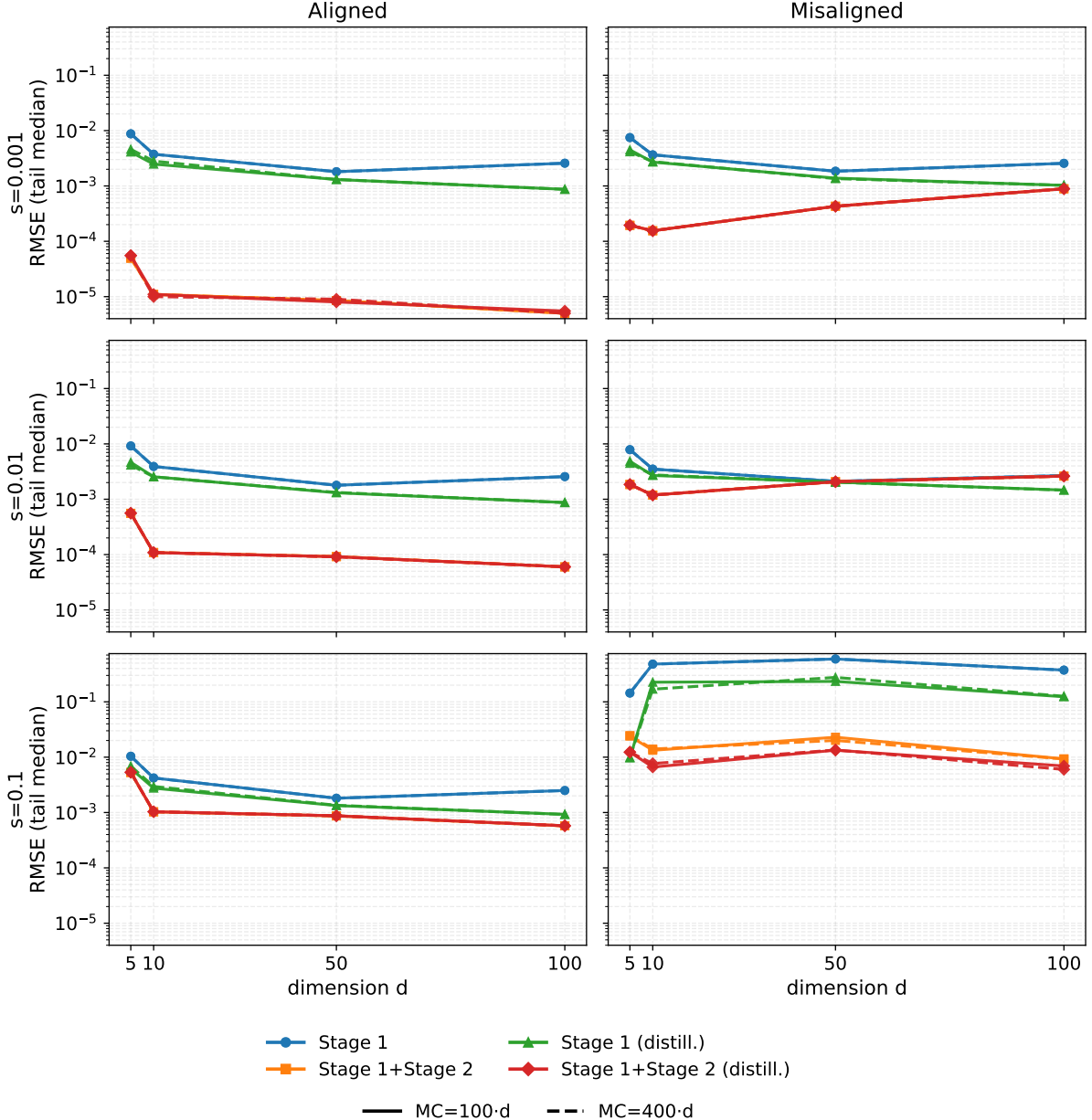


Figure 2: Decision-time Euclidean RMSE at $t = 0$ versus dimension d (log scale), summarized by a *tail median* over the late-training window. Concretely, for each condition we take the median RMSE over the last evaluation snapshots recorded during training. Rows: uncertainty magnitude $s \in \{10^{-3}, 10^{-2}, 10^{-1}\}$. Columns: aligned vs. misaligned geometry. Curves compare Stage 1 (deployable) and Stage 2 (post-hoc projection), with and without interactive distillation. Solid vs. dashed lines correspond to MC base ($100 \cdot d$) vs. high ($400 \cdot d$) trajectory budgets.

non-monotone and noisy RMSE curves, we summarize each condition by a robust *tail median*: the median RMSE over the final evaluation snapshots in the late-training window. Unless stated otherwise, the projection/teacher direction uses the p_θ aggregation (Section 3.2).

What is compared in Figure 2. Stage 1 (PG-DPO; Section 3.1) trains a deployable θ -blind policy π_φ by maximizing \hat{J} via pathwise gradients. Stage 2 (P-PGDPO; Section 3.2) applies a q -aggregated Pontryagin projection to a Stage 1 checkpoint; we use the residual form of Section F.1. Interactive distillation (Section F.2) treats the Stage 2 projected control as a teacher signal and amortizes it back into a deployable Stage 1 policy network.

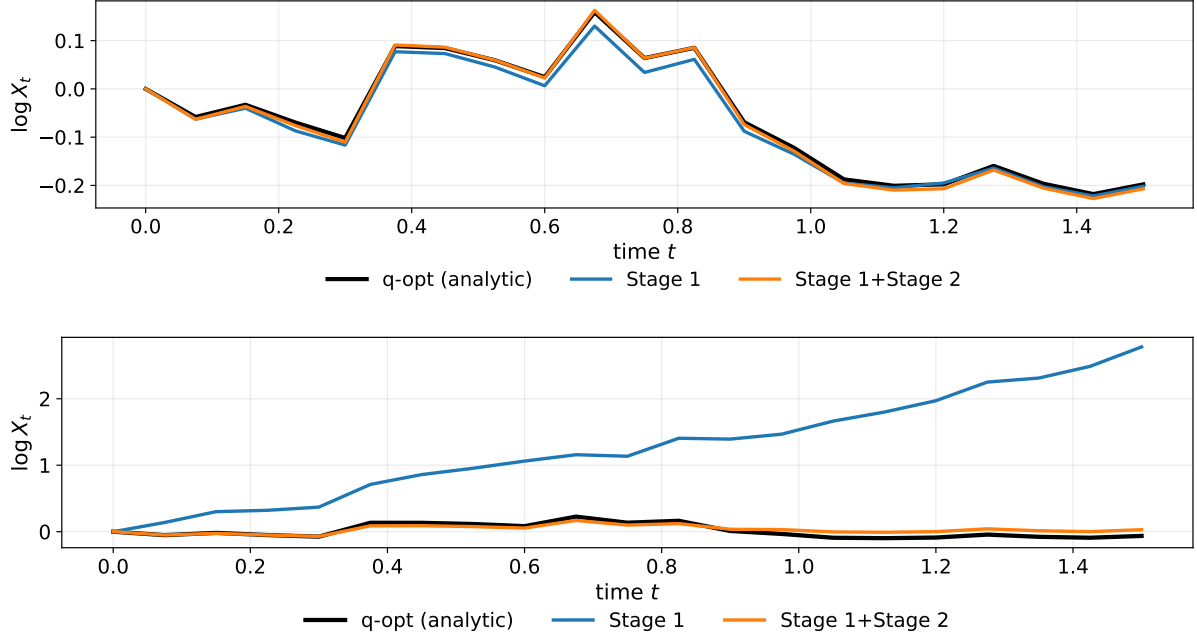


Figure 3: Pathwise sanity check at $d = 100$ under common random numbers. Black: analytic Gaussian constant-fraction benchmark evaluated with the remaining horizon $\tau = T - t$ (fixed q). Blue: Stage 1 PG-DPO. Orange: on-the-fly Stage 2 P-PGDPO teacher (computed via Monte Carlo projection at visited states). Top/bottom: aligned/misaligned.

Thus Figure 2 separates *projection quality* (Stage 2: post-hoc projected, still θ -blind) from *amortized deployable quality* (Stage 1 distilled: single forward pass).

Stage 2 projection versus amortization: scaling with dimension. For the **aligned geometry**, small and moderate uncertainty ($s = 10^{-3}, 10^{-2}$) yield a sharp Stage 2 reduction in decision-time error across all tested dimensions, bringing RMSE down to the 10^{-5} – 10^{-4} range, while Stage 1 policies remain around 10^{-3} . Interactive distillation consistently improves the deployable policy (Stage 1 (distill.) below Stage 1) while leaving Stage 2 essentially unchanged, confirming the intended division of labor: Stage 2 supplies a structured stationarity-correction signal, and distillation reduces the policy-class approximation/optimization gap by injecting that signal into π_φ .

In contrast, under the **misaligned geometry** the picture becomes more heterogeneous. For small to moderate uncertainty ($s = 10^{-3}, 10^{-2}$), Stage 2 still improves decision-time RMSE at small d , but its advantage shrinks with dimension and can approach the 10^{-3} level by $d = 100$. For the largest uncertainty scale ($s = 10^{-1}$), Stage 1 becomes markedly less reliable, whereas Stage 2 remains substantially better, indicating that projection can act as a stabilizing correction even when end-to-end learning is stressed. Across settings, the base and high MC budgets tend to yield similar tail-median RMSE curves, suggesting that linear-in- d scaling of simulation budgets is sufficient for stable comparisons in this benchmark.

Mechanism: why misalignment can reduce projection gains. To explain when and why the projection gains shrink, we analyze Stage 2 diagnostic statistics reported in Appendix G; see Figures 5–8. The diagnostics indicate that the degradation under misalignment is driven primarily by increased stationarity residuals and curvature mismatch, rather than by catastrophic denominator sign failures: (i) the Stage 2 residual norm grows with dimension and becomes especially large in the hardest misaligned regime, (ii) the projection denominator magnitude stays away from zero at typical quantiles, and (iii) the bad-sign fraction remains negligible, while (iv) the effective curvature statistic κ stays near the nominal $1/\gamma$ reference in easy regimes but

can deviate substantially in the hardest misaligned/high-uncertainty setting. These patterns are consistent with the geometric explanation: when P and Σ do not commute, the inverse operations implicit in projection mix uncertainty directions that are poorly aligned with risk directions, which can amplify estimation noise in the projected correction as d grows.

Pathwise sanity check. Figure 3 complements the decision-time RMSE with a trajectory-level view under common random numbers. In the aligned case, the on-the-fly Stage 2 teacher tracks the analytic q -reference closely along a realized path and reduces the deviation $\Delta \log X_t$ relative to the warm Stage 1 policy. In the misaligned case, the teacher can deviate more noticeably under the same common-noise protocol, mirroring the reduced projection advantage in the hardest regimes of Figure 2 and motivating amortization/reliability mechanisms in interactive distillation.

4.3 A strong RL baseline: PPO, and why it falls short in our benchmark

Why include PPO, and how we match the setting. Proximal Policy Optimization (PPO) is a widely used and robust model-free policy-gradient baseline for continuous control (Schulman et al., 2017). We include PPO to answer a concrete question: can a generic, well-tuned model-free RL method recover the decision-time q -optimal θ -blind allocation in our high-dimensional drift-uncertainty benchmark under comparable simulation budgets? This comparison is especially informative in our static Gaussian benchmark because the target decision-time rule is structurally simple (constant and available in closed form), so performance gaps primarily reflect optimization difficulty and credit assignment rather than policy-class expressiveness.

Since classical HJB solvers and value-function-based deep PDE surrogates are not practical baselines in the high-dimensional uncertain regime targeted here (Section B), PPO serves as a strong *simulation-only* comparator that operates on the same sampled trajectories without exploiting value-function PDE structure. For a fair comparison, PPO is trained on the same Euler simulator and time discretization as our PG–DPO pipeline, under the same deployability restriction (the policy never observes the latent θ), and under the same terminal-utility objective. We match simulation budgets at the level of total environment interactions (simulated trajectories \times time steps); implementation and PPO tuning details are deferred to the appendix and code release.

Empirical outcome. Table 1 shows that PPO remains far from the analytic decision-time q -reference across essentially all conditions, with RMSE typically on the order of 10^{-1} . In contrast, the Pontryagin-based pipeline attains substantially smaller errors: in aligned regimes Stage 2 projection reaches the 10^{-5} – 10^{-4} range for small and moderate uncertainty, while in misaligned regimes the projection advantage narrows but remains systematic. Distillation improves the *deployable* Stage 1 policy relative to basic PG–DPO, but does not eliminate the remaining gap to the post-hoc projection, consistent with the amortization interpretation in Section 4.2.

Why PPO underperforms in this benchmark. The gap is not evidence that PPO is intrinsically weak; rather, it reflects that our benchmark stresses regimes where a generic likelihood-ratio policy gradient is statistically disadvantaged compared to pathwise/adjoint-based updates.

Terminal-reward credit assignment. With terminal utility as the only reward signal, PPO faces a long-horizon credit-assignment problem: most intermediate transitions carry zero reward, so advantage estimates inherit high variance and weak learning signals, especially in higher dimensions.

One contributor is *terminal-reward credit assignment*: with terminal utility as the only reward signal, most intermediate transitions carry no direct learning signal, so advantage estimates become noisy and the gradient signal weakens as the horizon and dimension grow. A second contributor is *high-dimensional action noise and variance scaling*: in continuous control, exploration is typically implemented through stochastic policies (e.g., diagonal Gaussians), and

s	Method	Aligned				Misaligned			
		$d = 5$	10	50	100	$d = 5$	10	50	100
10^{-3}	Stage 1 (Basic)	8.76×10^{-3}	3.74×10^{-3}	1.81×10^{-3}	2.58×10^{-3}	7.49×10^{-3}	3.65×10^{-3}	1.85×10^{-3}	2.56×10^{-3}
	Stage 1+Stage 2 (Basic)	4.95×10^{-5}	1.10×10^{-5}	8.50×10^{-6}	5.00×10^{-6}	1.94×10^{-4}	1.55×10^{-4}	4.30×10^{-4}	8.89×10^{-4}
	Stage 1 (Distill.)	4.10×10^{-3}	2.48×10^{-3}	1.31×10^{-3}	1.70×10^{-3}	4.49×10^{-3}	2.70×10^{-3}	1.38×10^{-3}	1.02×10^{-3}
	Stage 1+Stage 2 (Distill.)	5.55×10^{-5}	1.10×10^{-5}	8.00×10^{-6}	5.50×10^{-6}	1.95×10^{-4}	1.55×10^{-4}	4.30×10^{-4}	8.89×10^{-4}
	PPO (baseline)	2.76×10^{-1}	1.14×10^{-1}	1.39×10^{-1}	1.67×10^{-1}	2.87×10^{-1}	8.25×10^{-2}	1.51×10^{-1}	1.69×10^{-1}
10^{-2}	Stage 1 (Basic)	9.19×10^{-3}	3.91×10^{-3}	1.79×10^{-3}	2.57×10^{-3}	7.87×10^{-3}	3.50×10^{-3}	2.11×10^{-3}	2.68×10^{-3}
	Stage 1+Stage 2 (Basic)	5.57×10^{-4}	1.09×10^{-4}	9.20×10^{-5}	6.00×10^{-5}	1.85×10^{-3}	1.19×10^{-3}	2.07×10^{-3}	2.62×10^{-3}
	Stage 1 (Distill.)	4.64×10^{-3}	2.55×10^{-3}	1.31×10^{-3}	1.80×10^{-3}	4.86×10^{-3}	2.69×10^{-3}	2.04×10^{-3}	1.46×10^{-3}
	Stage 1+Stage 2 (Distill.)	5.60×10^{-4}	1.09×10^{-4}	9.15×10^{-5}	6.00×10^{-5}	1.85×10^{-3}	1.19×10^{-3}	2.07×10^{-3}	2.62×10^{-3}
	PPO (baseline)	3.00×10^{-1}	7.88×10^{-2}	1.50×10^{-1}	1.58×10^{-1}	2.58×10^{-1}	8.99×10^{-2}	1.59×10^{-1}	1.38×10^{-1}
10^{-1}	Stage 1 (Basic)	1.04×10^{-2}	4.21×10^{-3}	1.81×10^{-3}	2.50×10^{-3}	1.44×10^{-1}	4.81×10^{-1}	5.94×10^{-1}	3.74×10^{-1}
	Stage 1+Stage 2 (Basic)	5.29×10^{-3}	1.03×10^{-3}	8.68×10^{-4}	5.76×10^{-4}	2.40×10^{-2}	1.33×10^{-2}	2.29×10^{-2}	9.31×10^{-3}
	Stage 1 (Distill.)	6.23×10^{-3}	2.76×10^{-3}	1.33×10^{-3}	1.53×10^{-3}	9.67×10^{-3}	2.26×10^{-1}	2.34×10^{-1}	1.24×10^{-1}
	Stage 1+Stage 2 (Distill.)	5.33×10^{-3}	1.03×10^{-3}	8.73×10^{-4}	5.76×10^{-4}	1.23×10^{-2}	6.63×10^{-3}	1.34×10^{-2}	6.93×10^{-3}
	PPO (baseline)	2.70×10^{-1}	9.65×10^{-2}	1.55×10^{-1}	1.78×10^{-1}	2.78×10^{-1}	8.84×10^{-2}	1.47×10^{-1}	1.77×10^{-1}

Table 1: Decision-time Euclidean RMSE at $t = 0$ (tail median over the late-training window; last six evaluation snapshots), computed using the common Euclidean-norm RMSE definition (71). Stage 1 rows report the deployable policy output. Stage 1+Stage 2 rows report the post-hoc P-PGDPO projection (residual form). “Distill.” rows correspond to the amortized deployable policy trained via interactive distillation. PPO is a model-free baseline trained under the same benchmark setting (same simulator, horizon $T = 1.5$, and θ -blind restriction). **Bold** entries indicate the best (lowest) RMSE among the five methods for each (s, d) and geometry.

as d increases the effective exploration noise and likelihood-ratio gradient variance can inflate rapidly, making it difficult to consistently recover the precise constant-fraction structure of the q -optimal θ -blind rule under fixed simulation budgets.

In contrast, Stage 1 exploits backpropagation through the differentiable simulator (pathwise gradients), and Stage 2 leverages the affine-in-control Pontryagin structure through a q -aggregated projection, replacing a noisy high-dimensional policy-gradient update by a structured stationarity correction that is tailored to the θ -blind *ex ante* objective.

5 Recovering Intertemporal Hedging Demand in Factor-Driven Markets

Sections 4 stressed *scaling* under static drift uncertainty, where the target q -reference is time-homogeneous and largely myopic. Here we shift the focus to an *economic* target: recovering the *intertemporal hedging demand* induced by factor-driven investment opportunities when return shocks are correlated with factor shocks (Campbell and Viceira, 2002; Xia, 2001).

We adopt the mean-reverting Gaussian premium benchmark of Section 2.3.2. At decision time ($t = 0$), the investor is assumed to have access only to an interval/posterior uncertainty description $q(dy)$ for the initial premium state Y_0 (e.g., $Y_0 \sim \mathcal{N}(m_0, P_0)$), and we restrict attention to *deployable* Y -blind policies that depend only on observable wealth and time-to-go. When return and factor shocks are correlated ($\rho \neq 0$), the analytic OU decision-time reference (43) contains the cross term $M_{\text{cross}}(\tau)$ (with $\tau := T - t$) that encodes intertemporal hedging demand.

We evaluate the two-stage PG–DPO / q -aggregated Pontryagin projection pipeline (and interactive distillation) against a model-free PPO baseline, all under the same Y -blind deployability restriction. Performance is measured by decision-time RMSE at $t = 0$ relative to the analytic constant-portfolio OU reference (43).

5.1 Experimental setting

Decision-time interval/posterior estimate for Y_0 and deployability. Throughout this section, all reported policies are *deployable and Y -blind*: the control is a function of observable wealth and time-to-go only, and never takes as input (i) a point estimate of Y_0 , (ii) the realized initial premium Y_0 , or (iii) the factor path (Y_t) (including the PPO baseline). At deployment, the investor is assumed to have access only to an uncertainty description $q(dy)$ for Y_0 (interval/posterior output of an external estimation pipeline), and commits to a single policy optimized *ex ante* under $Y_0 \sim q$ (without filtering/updating over $[0, T]$).

The latent premium factor is sampled and propagated *only inside the simulator* to generate trajectories and to form Monte Carlo averages used by the stage 2 projection (and by the teacher in distillation). Any Y -indexed quantities are used only for offline evaluation and diagnostics.

OU premium market with a hedging channel. We adopt the OU premium benchmark of Section 2.3.2. To avoid a notational clash with other uses of κ elsewhere in the paper, we denote the OU mean-reversion rate by κ_Y in this section. Let $Y_t \in \mathbb{R}^m$ be a mean-reverting premium factor and $R_t \in \mathbb{R}^d$ the risky excess returns:

$$\begin{aligned} dY_t &= \kappa_Y(\bar{y} - Y_t) dt + \Xi dW_t^Y, \quad Y_0 \sim \mathcal{N}(m_0, P_0), \\ dR_t &:= \frac{dS_t}{S_t} - r\mathbf{1} dt = BY_t dt + \Sigma^{1/2} dW_t, \\ d\langle W, W^Y \rangle_t &= \rho dt. \end{aligned}$$

Here $\rho \in \mathbb{R}^{d \times m}$ denotes the instantaneous return–factor shock correlation matrix, satisfying the feasibility condition $\rho^\top \rho \preceq I_m$. A nonzero ρ induces intertemporal hedging demand and enters

the CRRA decision-time reference through the cross-covariance term $M_{\text{cross}}(\tau)$ in (43), where $\tau := T - t$ is time-to-go (so at decision time $t = 0$, $\tau = T$). When $\rho = 0$ (independent return and factor shocks), the hedging channel vanishes ($M_{\text{cross}}(\tau) = 0$) and the reference reduces to the independence-case benchmark.

Decision-time uncertainty geometry for $Y_0 \sim \mathcal{N}(m_0, P_0)$. We control the magnitude of decision-time estimation uncertainty by a scalar $s_0 > 0$ and construct P_0 from an identification-motivated baseline

$$\tilde{P}_0 := (B^\top \Sigma^{-1} B)^{-1} \in \mathbb{R}^{m \times m}.$$

We consider two geometries. In the *aligned* case, we keep the principal directions of \tilde{P}_0 and rescale it so that the average marginal variance equals s_0 :

$$P_0^{\text{aligned}}(s_0) := \frac{s_0 m}{\text{tr}(\tilde{P}_0)} \tilde{P}_0, \quad (72)$$

so that $\text{tr}(P_0^{\text{aligned}})/m = s_0$. In the *misaligned* case, we preserve the eigenvalue spectrum of \tilde{P}_0 but randomize its eigenvectors via an orthogonal rotation: letting $\tilde{P}_0 = U \text{diag}(\lambda) U^\top$ be an eigen-decomposition and drawing an orthogonal matrix R (e.g., Haar), we define

$$P_0^{\text{misaligned}}(s_0) := \frac{s_0 m}{\text{tr}(\tilde{P}_0)} U R \text{diag}(\lambda) R^\top U^\top, \quad (73)$$

which matches the same trace normalization while rotating the uncertainty directions away from those of \tilde{P}_0 . We sweep $s_0 \in \{10^{-3}, 10^{-2}, 10^{-1}\}$ under both aligned and misaligned P_0 .

Two-stage solver, amortization, and evaluation protocol. We use the two-stage pipeline of Section 3. Stage 1 trains a deployable policy by stochastic gradient ascent using pathwise/BPTT gradients (Section 3.1). Stage 2 applies the q -aggregated Pontryagin projection computed under a warm-up policy (Section 3.2), implemented in the residual/control-variate form (Section F.1). Interactive distillation amortizes the projected teacher into a fast deployable policy network (Section F.2). As a model-free baseline, we also train a PPO policy under the same Y -blind observation restriction and report its decision-time full RMSE in Table 2.

We sweep $d \in \{5, 10, 50, 100\}$ (one fixed market instance per d , following the same market-generation protocol used in Section 4), train for 5000 epochs, and evaluate every 100 epochs. We evaluate the decision-time action at $t = 0$ (i.e., $\tau = T$) and report RMSE to the analytic constant-portfolio OU reference (43).

Unless stated otherwise we set $\gamma = 2$, $r = 0.03$, $\kappa_Y = 1.0$, $\xi_{\text{scale}} = 0.25$, and a correlation *magnitude* $\rho_0 = 0.5$. We instantiate the model parameters as follows: (i) we take $\Xi = \xi_{\text{scale}} I_m$, (ii) we implement the return-factor correlation by choosing a matrix $\rho = \rho_0 Q$ with $Q \in \mathbb{R}^{d \times m}$ having orthonormal columns ($Q^\top Q = I_m$), ensuring $\rho^\top \rho = \rho_0^2 I_m \preceq I_m$. (A simple choice is $Q = [I_m; 0] \in \mathbb{R}^{d \times m}$ when $m \leq d$; any fixed orthonormal-column Q yields an equivalent correlation magnitude.) We fix the horizon to $T = 1.5$ in this section.

In addition to the full allocation error, we use the myopic+hedging decomposition induced by the OU structure, and report component-wise diagnostics for the projected (Stage 2) rules. To reduce noise from stochastic optimization, for each condition we summarize each metric by a *tail median* over the last six evaluation checkpoints.

5.2 Results: hedging-demand recovery, amortization, and robustness to decision-time uncertainty

Metrics and diagnostics. Table 2 reports the full decision-time RMSE at $t = 0$ for all deployable policies, including the PPO baseline. To isolate the economic hedging channel, we use the OU-induced decomposition of the analytic reference

$$\pi^{\text{ref}}(\tau) = \pi^{\text{myo}}(\tau) + \pi^{\text{hedge}}(\tau),$$

s_0	Method	Aligned P_0				Misaligned P_0			
		$d = 5$	10	50	100	$d = 5$	10	50	100
10^{-3}	Stage 1 (Basic)	6.31×10^{-3}	5.19×10^{-3}	4.01×10^{-3}	3.54×10^{-3}	6.11×10^{-3}	5.40×10^{-3}	3.87×10^{-3}	3.62×10^{-3}
	Stage 1+Stage 2 (Basic)	4.71×10^{-5}	5.10×10^{-5}	1.39×10^{-4}	1.56×10^{-4}	5.12×10^{-5}	5.11×10^{-5}	1.35×10^{-4}	1.57×10^{-4}
	Stage 1 (Distill.)	2.46×10^{-3}	3.57×10^{-3}	3.58×10^{-3}	3.22×10^{-3}	3.51×10^{-3}	2.93×10^{-3}	3.56×10^{-3}	3.21×10^{-3}
	Stage 1+Stage 2 (Distill.)	4.43×10^{-5}	5.39×10^{-5}	1.37×10^{-4}	1.42×10^{-4}	4.36×10^{-5}	5.48×10^{-5}	1.41×10^{-4}	1.44×10^{-4}
	PPO (baseline)	7.78×10^{-2}	1.03×10^{-1}	4.20×10^0	2.41×10^0	8.96×10^{-2}	9.28×10^{-2}	4.37×10^0	2.46×10^0
10^{-2}	Stage 1 (Basic)	5.61×10^{-3}	4.83×10^{-3}	3.83×10^{-3}	3.50×10^{-3}	6.17×10^{-3}	4.89×10^{-3}	3.89×10^{-3}	3.57×10^{-3}
	Stage 1+Stage 2 (Basic)	5.03×10^{-5}	4.54×10^{-5}	1.45×10^{-4}	1.75×10^{-4}	4.99×10^{-5}	5.96×10^{-5}	1.54×10^{-4}	1.75×10^{-4}
	Stage 1 (Distill.)	3.08×10^{-3}	3.16×10^{-3}	3.53×10^{-3}	3.21×10^{-3}	2.84×10^{-3}	3.97×10^{-3}	3.68×10^{-3}	3.21×10^{-3}
	Stage 1+Stage 2 (Distill.)	4.48×10^{-5}	5.11×10^{-5}	1.47×10^{-4}	1.56×10^{-4}	4.63×10^{-5}	6.31×10^{-5}	1.54×10^{-4}	1.57×10^{-4}
	PPO (baseline)	7.30×10^{-2}	9.15×10^0	4.27×10^0	2.43×10^0	8.02×10^{-2}	7.75×10^0	4.47×10^0	2.53×10^0
10^{-1}	Stage 1 (Basic)	6.93×10^{-3}	4.53×10^{-3}	3.96×10^{-3}	3.47×10^{-3}	6.09×10^{-3}	4.17×10^{-3}	3.97×10^{-3}	3.56×10^{-3}
	Stage 1+Stage 2 (Basic)	5.50×10^{-5}	4.16×10^{-5}	2.63×10^{-4}	2.97×10^{-4}	5.63×10^{-5}	2.44×10^{-4}	3.24×10^{-4}	3.29×10^{-4}
	Stage 1 (Distill.)	2.85×10^{-3}	3.70×10^{-3}	3.65×10^{-3}	3.28×10^{-3}	3.22×10^{-3}	3.08×10^{-3}	3.65×10^{-3}	3.18×10^{-3}
	Stage 1+Stage 2 (Distill.)	4.77×10^{-5}	5.50×10^{-5}	2.60×10^{-4}	2.88×10^{-4}	5.31×10^{-5}	2.46×10^{-4}	3.22×10^{-4}	3.21×10^{-4}
	PPO (baseline)	7.34×10^{-2}	1.00×10^{-1}	4.22×10^0	2.64×10^0	6.30×10^{-2}	1.08×10^{-1}	4.26×10^0	2.46×10^0

Table 2: Decision-time RMSE at $t = 0$ in the OU premium benchmark (tail median over the last six evaluation checkpoints), sweeping the decision-time uncertainty scale s_0 in $Y_0 \sim \mathcal{N}(m_0, P_0)$ under both aligned (72) and misaligned (73) geometries. Stage 1 reports the deployable PG–DPO policy output. Stage 1+Stage 2 reports the post-hoc q -aggregated Pontryagin projection (residual form (104)) computed under the corresponding warm policy. “Distill.” rows use interactive distillation (Section F.2) to amortize the projected teacher. RMSE is computed identically for all methods (no method-specific or post-hoc scale correction). The PPO baseline is frequently unstable in this terminal-only, Y -blind setting; very large entries (e.g., $s_0 = 10^{-2}$, $d = 10$) reflect genuine training divergence rather than typographical error.

s_0	Method	$d = 5$	10	50	100
Aligned P_0					
10^{-3}	Stage 1+Stage 2 (Basic)	4.59×10^{-5}	4.87×10^{-5}	1.37×10^{-4}	1.55×10^{-4}
	Stage 1+Stage 2 (Distill.)	4.39×10^{-5}	5.25×10^{-5}	1.37×10^{-4}	1.42×10^{-4}
10^{-2}	Stage 1+Stage 2 (Basic)	4.98×10^{-5}	4.47×10^{-5}	1.44×10^{-4}	1.74×10^{-4}
	Stage 1+Stage 2 (Distill.)	4.43×10^{-5}	4.95×10^{-5}	1.47×10^{-4}	1.55×10^{-4}
10^{-1}	Stage 1+Stage 2 (Basic)	5.27×10^{-5}	3.99×10^{-5}	2.60×10^{-4}	2.95×10^{-4}
	Stage 1+Stage 2 (Distill.)	4.72×10^{-5}	5.36×10^{-5}	2.58×10^{-4}	2.86×10^{-4}
Misaligned P_0					
10^{-3}	Stage 1+Stage 2 (Basic)	5.00×10^{-5}	4.87×10^{-5}	1.34×10^{-4}	1.57×10^{-4}
	Stage 1+Stage 2 (Distill.)	4.30×10^{-5}	5.33×10^{-5}	1.40×10^{-4}	1.43×10^{-4}
10^{-2}	Stage 1+Stage 2 (Basic)	4.93×10^{-5}	5.65×10^{-5}	1.53×10^{-4}	1.75×10^{-4}
	Stage 1+Stage 2 (Distill.)	4.56×10^{-5}	6.09×10^{-5}	1.53×10^{-4}	1.56×10^{-4}
10^{-1}	Stage 1+Stage 2 (Basic)	5.45×10^{-5}	1.55×10^{-4}	3.19×10^{-4}	3.28×10^{-4}
	Stage 1+Stage 2 (Distill.)	5.20×10^{-5}	1.57×10^{-4}	3.13×10^{-4}	3.20×10^{-4}

Table 3: Decision-time RMSE at $t = 0$ for the *hedging component* of the OU decision-time reference, evaluated on the post-hoc projected (Stage 2) policies (tail median over the last six evaluation checkpoints). We use the decomposition $\pi^{\text{ref}}(\tau) = \pi^{\text{myo}}(\tau) + \pi^{\text{hedge}}(\tau)$ where π^{myo} is the $\rho = 0$ reference and π^{hedge} is the residual ρ -dependent term (cf. (43)). Component-wise diagnostics are reported for Stage 2 since Stage 1 and PPO do not explicitly output a compatible myopic/hedging split under our protocol.

where π^{myo} is the independence-case reference obtained by setting $\rho = 0$ (equivalently, dropping $M_{\text{cross}}(\tau)$ in (43)), and $\pi^{\text{hedge}} := \pi^{\text{ref}} - \pi^{\text{myo}}$ is the residual ρ -dependent term. We report the hedging-component RMSE for the projected (Stage 2) rules in Table 3; the myopic-component RMSE and hedging-direction cosine similarity are deferred to Appendix H. Since Stage 1 and PPO do not expose a compatible myopic/hedging split under our diagnostic protocol, component-wise diagnostics are reported only for Stage 2.

Projection and economic hedging-demand recovery. Across all d and s_0 , the post-hoc Pontryagin projection (Stage 1+Stage 2) substantially reduces decision-time RMSE relative to the deployable Stage 1 policy (Table 2). For example, under aligned P_0 with $s_0 = 10^{-3}$ and $d = 100$, Stage 1 attains 3.54×10^{-3} whereas Stage 1+Stage 2 achieves 1.56×10^{-4} . The component-wise diagnostics indicate that the remaining discrepancy is largely driven by the hedging channel: in the same setting, the hedging RMSE is 1.55×10^{-4} (Basic) and 1.42×10^{-4} (Distill.) (Table 3), while the myopic RMSE is an order of magnitude smaller (Appendix Table 4). This pattern is consistent with the economic mechanism in this benchmark: once the (mostly) myopic component is captured, the dominant remaining challenge is to recover the intertemporal hedge induced by correlated return-factor shocks.

Amortization, robustness, and the PPO baseline. Interactive distillation improves the *deployable* Stage 1 policy relative to the basic PG–DPO run, while the most accurate object remains the post-hoc projected policy (Table 2). This matches the intended division of labor in Section F: Stage 2 provides a structured stationarity-correction signal through the aggregated Pontryagin projection, and distillation amortizes that correction into a single forward pass, up to policy-class approximation limits.

As the decision-time uncertainty scale s_0 increases, both the full RMSE and the hedging-component RMSE increase, with the most visible degradation at $s_0 = 10^{-1}$, especially at larger

dimensions (Tables 2–3). Misalignment has a limited effect for small and moderate uncertainty scales, but can induce noticeable deterioration in the hardest settings, where the direction-of-hedge diagnostic can also weaken (Appendix Table 5).

Finally, the PPO baseline remains far from the analytic OU reference under the same Y -blind deployability restriction, and can be unstable in this terminal-only setting (Table 2). This is consistent with PPO facing a difficult credit-assignment problem under latent-factor heterogeneity, in contrast to the pathwise-sensitivity and affine-in-control correction exploited by our two-stage pipeline. Since PPO does not provide a compatible myopic/hedging decomposition under our evaluation protocol, we include it only in the full-RMSE table.

6 Conclusion

We studied continuous-time portfolio choice in diffusion markets whose coefficients are estimated and therefore subject to statistical uncertainty (Section 2.1). We model this uncertainty by an exogenous law $q(d\theta)$ over a latent parameter θ that is drawn once at time 0 and remains fixed over the investment horizon, while the investor must deploy a single θ -blind Markov feedback policy evaluated under an ex-ante CRRA objective (Remark 1, Section 2.1). This information structure shifts the relevant optimality notion from θ -conditional (full-information) criticality to a q -aggregated Pontryagin first-order condition that is enforceable within the deployable θ -blind policy class (Section 2.2, Theorem 1).

Methodologically, we extended Pontryagin–Guided Direct Policy Optimization (PG–DPO) to the latent-parameter setting by sampling θ only inside the simulator and computing exact discrete-time gradients via BPTT (Section 3.1), and we leveraged the BPTT–PMP correspondence to extract the costate objects needed for structured control updates (Theorem 2). Building on the q -aggregated stationarity, we proposed uncertainty-aware projected PG–DPO (P–PGDPO), which aggregates Monte Carlo Pontryagin quantities across $\theta \sim q$ and projects them onto the deployable first-order condition to obtain a single θ -blind rule (Section 3.2). We established a residual-based ex-ante policy-gap bound under local stability of the aggregated projection map, with discretization and Monte Carlo errors made explicit (Theorem 3). In experiments, projection provides the dominant gains—improving stability and decision-time accuracy in high-dimensional drift-uncertainty scaling tests and recovering intertemporal hedging demand in factor-driven markets—while interactive distillation amortizes projection into a fast deployable network (Sections 4 and 5; Section F).

Several extensions are natural. A first direction is to allow time-varying uncertainty descriptions q_t (e.g., produced by an external filter) and connect the present fixed- q projection to belief-aware decision rules (Remark 2, Appendix A). A second direction is to incorporate realistic frictions and constraints (transaction costs, leverage and short-sale limits) and develop certified or regularized projection steps when mixed-moment estimation becomes fragile (Section B; Section 4.2; Appendix E.5). Finally, applying the framework to large cross-sectional datasets with modern estimation pipelines would further clarify the practical benefits of inference-agnostic, simulation-only optimization under parameter uncertainty (Section 1).

Acknowledgments

This work was supported by the National Research Foundation of Korea (NRF) grant funded by the Korea government (MSIT) (RS-2025-00562904).

References

- Baghery, F. and Øksendal, B. (2007). A maximum principle for stochastic control with partial information. *Stochastic Analysis and Applications*, 25(3):705–717. 2, A
- Barberis, N. (2000). Investing for the long run when returns are predictable. *The Journal of Finance*, 55(1):225–264. 1, 2.3.1, 2.3.1, 2.3.1, A, A
- Beck, C., E, W., and Jentzen, A. (2019). Machine learning approximation algorithms for high-dimensional fully nonlinear partial differential equations and second-order backward stochastic differential equations. *Journal of Nonlinear Science*, 29:1563–1619. 1, B, B.3
- Bellman, R. (1961). *Adaptive Control Processes: A Guided Tour*. Princeton University Press, Princeton, NJ. 1, B, B.2
- Bensoussan, A. and van Schuppen, J. H. (1985). Optimal control of partially observable stochastic systems with an exponential-of-integral performance index. *SIAM Journal on Control and Optimization*, 23(4):599–613. 1, 2.1, A, A, A, B, B.1, B.1
- Breiman, L. (1996). Bagging predictors. *Machine Learning*, 24(2):123–140. 2.1
- Campbell, J. Y. and Thompson, S. B. (2008). Predicting excess stock returns out of sample: Can anything beat the historical average? *The Review of Financial Studies*, 21(4):1509–1531. 1
- Campbell, J. Y. and Viceira, L. M. (2002). *Strategic asset allocation: portfolio choice for long-term investors*. Clarendon Lectures in Economic. 1, 2.3.2, 2.3.2, 2.3.2, 5
- Efron, B. (1979). Bootstrap methods: Another look at the jackknife. *The Annals of Statistics*, 7(1):1–26. 1, 2.1
- Efron, B. and Tibshirani, R. J. (1994). *An Introduction to the Bootstrap*. Chapman & Hall/CRC. 1, 2.1
- Fleming, W. H. and Soner, H. M. (2006). *Controlled Markov processes and viscosity solutions*, volume 25. Springer Science & Business Media. 1, 2.2, 2.2, B, B.2, B.4
- Goyal, A. and Welch, I. (2008). A comprehensive look at the empirical performance of equity premium prediction. *The Review of Financial Studies*, 21(4):1455–1508. 1
- Han, J., Jentzen, A., and E, W. (2018). Solving high-dimensional partial differential equations using deep learning. *Proceedings of the National Academy of Sciences*, 115(34):8505–8510. 1, B, B.3
- Haussmann, U. G. (1987). The maximum principle for optimal control of diffusions with partial information. *SIAM Journal on Control and Optimization*, 25(2):341–361. 2, A
- Huh, J., Jeon, J., Koo, H. K., and Lim, B. H. (2025a). Breaking the dimensional barrier: A pontryagin-guided direct policy optimization for continuous-time multi-asset portfolio. *arXiv preprint arXiv:2504.11116*. 1, 3.2, C, 3
- Huh, J., Jeon, J., Koo, H. K., and Lim, B. H. (2025b). Breaking the dimensional barrier for constrained dynamic portfolio choice. *Available at SSRN 5672251*. 1
- Kandel, S. and Stambaugh, R. F. (1996). On the predictability of stock returns: An asset-allocation perspective. *The Journal of Finance*, 51(2):385–424. 1, 2.3.1, 2.3.1

- Kushner, H. J. and Dupuis, P. (2001). *Numerical Methods for Stochastic Control Problems in Continuous Time*, volume 24 of *Stochastic Modelling and Applied Probability*. Springer, New York, NY, 2 edition. 1, B, B.2
- LeCun, Y. (1988). A theoretical framework for back-propagation. In Touretzky, D. S., Hinton, G. E., and Sejnowski, T. J., editors, *Proceedings of the 1988 Connectionist Models Summer School*, pages 21–28. Morgan Kaufmann, San Mateo, CA. CMU, Pittsburgh, PA. 1
- Li, X. and Tang, S. (1995). General necessary conditions for partially observed optimal stochastic controls. *Journal of Applied Probability*, 32(4):1118–1137. 2, A
- Maenhout, P. J. (2004). Robust portfolio rules and asset pricing. *The Review of Financial Studies*, 17(4):951–983. 1
- Merton, R. C. (1969). Lifetime portfolio selection under uncertainty: The continuous-time case. *The review of Economics and Statistics*, pages 247–257. 1, 2.3.1
- Merton, R. C. (1971). Optimum consumption and portfolio rules in a continuous-time model. *Journal of Economic Theory*, 3(4):373–413. 1, 2.3.1
- Pástor, Ľ. (2000). Portfolio selection and asset pricing models. *The Journal of Finance*, 55(1):179–223. 2.3.1, 2.3.1, 2.3.1, A, A
- Pham, H. (2009). *Continuous-time stochastic control and optimization with financial applications*, volume 61. Springer Science & Business Media. 1, 2.2, 2.2, B, B.2, B.4
- Pham, H. and Wei, X. (2017). Dynamic programming for optimal control of stochastic mckean–vlasov dynamics. *SIAM Journal on Control and Optimization*, 55(2):1069–1101. 1, 2.1, A, A, B, B.1, B.1
- Raissi, M., Perdikaris, P., and Karniadakis, G. E. (2019). Physics-informed neural networks: A deep learning framework for solving forward and inverse problems involving nonlinear partial differential equations. *Journal of Computational physics*, 378:686–707. 1, B, B.3
- Ross, S. A. (1976). The arbitrage theory of capital asset pricing. *Journal of Economic Theory*, 13(3):341–360. 4.1
- Schulman, J., Wolski, F., Dhariwal, P., Radford, A., and Klimov, O. (2017). Proximal policy optimization algorithms. 4.3
- Sirignano, J. and Spiliopoulos, K. (2018). Dgm: A deep learning algorithm for solving partial differential equations. *Journal of computational physics*, 375:1339–1364. 1, B, B.3
- van der Vaart, A. W. (1998). *Asymptotic Statistics*. Cambridge University Press. 1, 2.1
- Xia, Y. (2001). Learning about predictability: The effects of parameter uncertainty on dynamic asset allocation. *The Journal of Finance*, 56(1):205–246. 1, 2.3.2, 2.3.2, 2.3.2, 5, A, A
- Yong, J. and Zhou, X. Y. (1999). *Stochastic controls: Hamiltonian systems and HJB equations*, volume 43. Springer Science & Business Media. 1, 2.2, 2.2

A Online uncertainty updates: Kalman–Bucy filtering and a plug-in decision-time benchmark

Purpose and scope. Sections 2.3.1 and 2.3.2 focus on *decision-time* benchmarks in which an uncertainty description q is treated as given and the investor optimizes under the corresponding θ -blind deployability constraint. In practice, however, new data arrive and the uncertainty description is updated over time by an external estimation/filtering engine, a viewpoint that aligns with learning/estimation-risk portfolio choice and Bayesian decision-time formulations (Barberis, 2000; Pástor, 2000; Xia, 2001). This subsection records a simple linear–Gaussian example in which such an updated description q_t arises endogenously via a Kalman–Bucy filter (a canonical partially observed diffusion setting; see, e.g., Bensoussan and van Schuppen (1985); Pham and Wei (2017)), and then formalizes a *plug-in* workflow: at each decision time, treat the current uncertainty description q_t as given and compute a decision-time optimal control under that q_t . We emphasize that solving the fully optimal partial-observation (belief-state) control problem is *not* the goal of this paper; rather, we view the resulting q_t as an external input to decision-time optimization. In particular, our simulation-based Pontryagin-guided solvers developed later (Section 3) can be used as inner-loop engines that are refreshed whenever a new uncertainty description q_t becomes available.

A linear–Gaussian hidden-premium model (OU state, observed returns). We use a stylized linear–Gaussian counterpart of the mean-reverting premium setting, but now assume the premium factor is not directly observed. Let $Y_t \in \mathbb{R}^m$ be a latent premium factor following an OU dynamics

$$dY_t = K(\bar{y} - Y_t) dt + \Xi dW_t^Y, \quad Y_0 \sim \mathcal{N}(\hat{y}_0, P_0), \quad (74)$$

where $K \in \mathbb{R}^{m \times m}$ is stable, $\bar{y} \in \mathbb{R}^m$, and $\Xi \in \mathbb{R}^{m \times m}$. Risky assets satisfy

$$\frac{dS_t}{S_t} = r\mathbf{1} dt + BY_t dt + \Sigma^{1/2} dW_t, \quad \Sigma \in \mathbb{R}^{d \times d} \text{ s.p.d.}, \quad (75)$$

with $B \in \mathbb{R}^{d \times m}$. Equivalently, the investor observes the excess-return signal

$$dZ_t := \frac{dS_t}{S_t} - r\mathbf{1} dt = BY_t dt + \Sigma^{1/2} dW_t. \quad (76)$$

We write $\mathbb{F}^Z = (\mathcal{F}_t^Z)_{t \in [0, T]}$ for the filtration generated by $(Z_s)_{s \leq t}$. For clarity, we present the independent-noise case $W \perp W^Y$; the correlated-noise extension remains linear–Gaussian but leads to more cumbersome gain formulas.

Kalman–Bucy posterior $q_t = \mathcal{L}(Y_t \mid \mathcal{F}_t^Z)$. Under (74)–(76), the conditional law of the latent factor remains Gaussian:

$$q_t(dy) := \mathcal{L}(Y_t \mid \mathcal{F}_t^Z) = \mathcal{N}(\hat{Y}_t, P_t), \quad (77)$$

where (\hat{Y}_t, P_t) satisfy the Kalman–Bucy equations

$$d\hat{Y}_t = K(\bar{y} - \hat{Y}_t) dt + P_t B^\top \Sigma^{-1} (dZ_t - B\hat{Y}_t dt), \quad (78)$$

$$\dot{P}_t = KP_t + P_t K^\top + \Xi \Xi^\top - P_t B^\top \Sigma^{-1} B P_t, \quad P_0 \text{ given.} \quad (79)$$

Thus, even though the posterior q_t is a distribution-valued object, in this affine/Gaussian regime it is fully characterized by the finite-dimensional sufficient statistics (\hat{Y}_t, P_t) , with P_t evolving deterministically via (79); this is the prototypical setting in which belief-state control reduces to finite-dimensional sufficient statistics (Bensoussan and van Schuppen, 1985; Pham and Wei, 2017).

From a posterior on Y_t to a Gaussian uncertainty description for decision-time optimization. To mirror the decision-time perspective of the OU benchmark, we consider the remaining-horizon time-averaged premium

$$\bar{\theta}_{t,T} := \frac{1}{T-t} \int_t^T B Y_s ds \in \mathbb{R}^d, \quad \tau := T-t. \quad (80)$$

For the OU dynamics (74), one has the decomposition

$$\int_t^T Y_s ds = \tau \bar{y} + K^{-1}(I - e^{-K\tau})(Y_t - \bar{y}) + \int_t^T K^{-1}(I - e^{-K(T-u)})\Xi dW_u^Y. \quad (81)$$

Conditioning on \mathcal{F}_t^Z , the random variable Y_t is distributed as $\mathcal{N}(\hat{Y}_t, P_t)$ by (77), while the future increments $(W_u^Y - W_t^Y)_{u \geq t}$ are independent of \mathcal{F}_t^Z in the independent-noise case. Hence $\bar{\theta}_{t,T} \mid \mathcal{F}_t^Z$ is Gaussian:

$$\bar{\theta}_{t,T} \mid \mathcal{F}_t^Z \sim \mathcal{N}(m_{t,T}, P_{t,T}), \quad m_{t,T} := \frac{B m_I(t, T)}{\tau}, \quad P_{t,T} := \frac{1}{\tau^2} B C_I(t, T) B^\top, \quad (82)$$

where

$$m_I(t, T) := \tau \bar{y} + K^{-1}(I - e^{-K\tau})(\hat{Y}_t - \bar{y}), \quad (83)$$

$$C_I(t, T) := K^{-1}(I - e^{-K\tau}) P_t (I - e^{-K\tau})^\top K^{-\top} + \int_0^\tau K^{-1}(I - e^{-Ks}) \Xi \Xi^\top (I - e^{-Ks})^\top K^{-\top} ds. \quad (84)$$

Equation (82) provides a concrete example of an *online-updated* Gaussian uncertainty description $q_{t,T} := \mathcal{L}(\bar{\theta}_{t,T} \mid \mathcal{F}_t^Z) = \mathcal{N}(m_{t,T}, P_{t,T})$.

A plug-in decision-time benchmark (receding-horizon fixed- $q_{t,T}$). Given $(m_{t,T}, P_{t,T})$ from (82), a simple decision-time rule is obtained by treating $q_{t,T}$ as fixed over the remaining horizon and applying the Gaussian constant-allocation benchmark of Section 2.3.1 with horizon τ :

$$\pi_t^{\text{plug}} := \left(\gamma \Sigma + (\gamma - 1)\tau P_{t,T} \right)^{-1} m_{t,T}. \quad (85)$$

One may interpret (85) as a *receding-horizon* decision-time policy driven by an externally updated uncertainty description, consistent with the general “update beliefs, then optimize” workflow used in Bayesian/learning-based portfolio choice (Barberis, 2000; Pástor, 2000; Xia, 2001).

Remarks (relation to belief-aware control). The plug-in rule (85) is intentionally decision-time: it conditions on the current uncertainty description and does not attempt to optimize over how the posterior will evolve. In the present paper, we therefore treat the uncertainty law as fixed at a decision time (either as a fixed q over a horizon, or as an externally updated sequence of inputs q_t that is *not* controlled by the agent), mirroring the decision-time perspective common in Bayesian/learning portfolio-choice studies (Barberis, 2000; Pástor, 2000; Xia, 2001). Even in linear-Gaussian regimes where the belief state is finite-dimensional, the *fully optimal* partial-observation portfolio problem would treat the belief state (here, (\hat{Y}_t, P_t)) as part of the controlled state and optimize the policy in that enlarged state space (Bensoussan and van Schuppen, 1985; Pham and Wei, 2017). Related necessary conditions under partial information can also be expressed via partial-observation maximum principles (Haussmann, 1987; Li and Tang, 1995; Baghery and Øksendal, 2007). Developing a belief-aware Pontryagin-guided policy optimizer that operates directly in (x, y, \hat{Y}, P) -space (or its sufficient-statistic analogues) is an important direction that we defer to future work.

B Why dynamic programming and deep PDE surrogates are not primary baselines under the θ -blind fixed- q interface

This appendix explains why we do *not* treat classical dynamic programming (DP/HJB) or value-function-based deep PDE surrogates (PINNs / deep BSDE methods) as practical baselines in the high-dimensional uncertain markets targeted in this paper. DP is conceptually sound in low-dimensional Markovian settings (Fleming and Soner, 2006; Pham, 2009), but two obstructions dominate in our regime: (i) value-function approaches require accurate *derivatives* (often including mixed sensitivities) to recover optimal portfolios, and this becomes prohibitive as dimension and nonlinearity grow; (ii) principled parameter uncertainty magnifies both the *state dimension* and the *aggregation* difficulties. These points are standard for grid-based HJB solvers (Bellman, 1961; Kushner and Dupuis, 2001) and remain relevant for modern deep PDE surrogates (Raissi et al., 2019; Sirignano and Spiliopoulos, 2018; Han et al., 2018; Beck et al., 2019), especially under partial information/belief-state formulations (Bensoussan and van Schuppen, 1985; Pham and Wei, 2017).

B.1 The value-function target for latent θ is a belief-state functional

Fixed- q ex-ante objective and θ -blind deployability. Our decision-time interface is

$$\sup_{\pi \in \mathcal{A}^{\text{blind}}} J(\pi) := \sup_{\pi \in \mathcal{A}^{\text{blind}}} \mathbb{E}_{\theta \sim q} [\mathbb{E}[U(X_T^\pi) \mid \theta]], \quad (86)$$

where $\theta \sim q$ is latent, fixed along each episode, and $\mathcal{A}^{\text{blind}}$ denotes admissible controls measurable with respect to the *observable* filtration (so the deployed policy cannot take θ as an input).

Why (t, X_t, Y_t) is not a closed DP state. In general, the observable history carries information about θ , so the continuation value at time t depends on the conditional law

$$q_t(\cdot) := \mathcal{L}(\theta \mid \mathcal{F}_t^{\text{obs}}), \quad (87)$$

not only on (t, X_t, Y_t) . This is the standard partially observed control phenomenon: DP becomes Markov only after augmenting the state by a belief (or a finite-dimensional sufficient statistic when available) (Bensoussan and van Schuppen, 1985; Pham and Wei, 2017).

Belief-state DP is infinite-dimensional under our interface. The principled DP value function is therefore a functional of a probability measure:

$$V(t, x, y, \mu) := \sup_{\pi \in \mathcal{A}^{\text{blind}}} \mathbb{E}^{t, x, y, \mu} [U(X_T^\pi)], \quad \mu \in \mathcal{P}(\Theta), \quad (88)$$

so the associated HJB equation is posed on a space of measures in general (Bensoussan and van Schuppen, 1985; Pham and Wei, 2017). Under our inference-agnostic interface, q need not belong to a conjugate family and we do not specify a filtering model that would keep q_t in a tractable finite-dimensional class. Consequently, a DP/PDE baseline would be forced to approximate V over an *infinite-dimensional* belief state, which is not the computational target of this paper.

B.2 Even with deterministic parameters, HJB solvers face a derivative bottleneck in high dimension

Classical HJB: curse of dimensionality and full nonlinearity. With deterministic parameters, DP leads to an HJB for $V(t, x, y)$ (Fleming and Soner, 2006; Pham, 2009). Grid-based

solvers scale exponentially in the state dimension (Bellman, 1961; Kushner and Dupuis, 2001). In portfolio problems with d assets and m factors, the natural state already has dimension $m+2$, so even modest discretizations require N^{m+2} grid points.

Moreover, realistic features (constraints, transaction costs, non-affine dynamics) typically yield *fully nonlinear* HJBs. Recovering the optimal portfolio from a value function also requires derivatives (schematically, in Merton-type problems)

$$\pi^*(t, x, y) \propto -\frac{V_x(t, x, y)}{V_{xx}(t, x, y)} \times (\text{risk model})^{-1} \times (\text{drift model}), \quad (89)$$

and in factor-driven settings intertemporal hedging demands are driven by mixed sensitivities (e.g. V_{xy}). Thus the numerical burden is not only approximating V but also obtaining stable *first/second/mixed* derivatives in high dimension.

B.3 Deep PDE surrogates remove grids but not the value-function derivative bottleneck

PINNs and deep BSDE methods replace grids with neural approximators trained on sampled points/paths (Raissi et al., 2019; Sirignano and Spiliopoulos, 2018; Han et al., 2018; Beck et al., 2019), but for fully nonlinear portfolio HJBs they remain value-function-based: they must implicitly learn high-dimensional gradients/Hessians and, crucially, mixed sensitivities that drive intertemporal hedging. In practice this can induce nonconvex and ill-conditioned training objectives (due to control suprema and nonlinear derivative dependence) and training signals that do not reliably control the specific derivative components needed for stable high-dimensional portfolio policies.

This is not a claim that deep PDE methods are “invalid”; rather, under our *high-dimensional* and θ -*blind* interface, they are not practical baselines relative to direct, simulation-only policy optimization methods.

B.4 Why θ -conditional value functions do not solve the θ -blind ex–ante problem

A natural alternative is to condition on θ and solve a family of full-information problems.

θ -conditional HJB. If θ were observed, the full-information value function V^θ solves

$$0 = \partial_t V^\theta(t, x, y) + \sup_{\pi \in \mathbb{R}^d} \left\{ \mathcal{L}^{\pi, \theta} V^\theta(t, x, y) \right\}, \quad V^\theta(T, x, y) = U(x), \quad (90)$$

for the controlled generator $\mathcal{L}^{\pi, \theta}$ (Fleming and Soner, 2006; Pham, 2009). This yields a θ -dependent optimizer $\pi^*(t, x, y, \theta)$, which is infeasible in our deployable θ -blind setting.

Supremum–expectation non-commutativity. More fundamentally, even perfect knowledge of the θ -conditional optimizer does not solve the θ -blind objective, because

$$\sup_{\pi \in \mathcal{A}^{\text{blind}}} \mathbb{E}_{\theta \sim q}[J(\pi, \theta)] \leq \mathbb{E}_{\theta \sim q} \left[\sup_{\pi} J(\pi, \theta) \right], \quad J(\pi, \theta) := \mathbb{E}[U(X_T^\pi) \mid \theta], \quad (91)$$

and the inequality is typically strict. The right-hand side corresponds to the (infeasible) θ -adaptive controller.

B.5 Why “sample θ only in the PDE loss” is mismatched to the ex-ante objective

One might try to train a single value network $V_\varphi(t, x, y)$ that does *not* take θ as input, and sample $\theta \sim q$ only inside a collocation/pathwise residual loss:

$$\min_{\varphi} \mathbb{E}_{\theta \sim q} \left[\left\| \text{HJB}_\theta(V_\varphi)(t, x, y) \right\|^2 \right], \quad (\text{schematic}) \quad (92)$$

where $\text{HJB}_\theta(\cdot)$ is the full-information HJB operator for parameter θ . This is appealing but generally mismatched to (86):

- Different θ impose different (often conflicting) optimality conditions at the same (t, x, y) , so there is generally no single V satisfying $\text{HJB}_\theta(V) = 0$ for many θ simultaneously.
- Minimizing an expected squared PDE residual (92) is not equivalent to maximizing expected terminal utility under θ -blind controls.
- Portfolio feedback rules are typically extracted through nonlinear operations on derivatives (ratios, inverses), so small value-function approximation errors can induce large control errors.

B.6 A toy calculation: $\mathbb{E}[\pi^*(\theta)] \neq \pi_q^*$ under CRRA

The aggregation issue is visible even in a one-asset Merton model with static latent drift. Let

$$\frac{dS_t}{S_t} = r dt + \theta dt + \sigma dW_t, \quad \theta \sim \mathcal{N}(m, p),$$

and restrict to constant fractions π over a remaining horizon τ . For CRRA utility $U(x) = x^{1-\gamma}/(1-\gamma)$ with $\gamma > 1$, the θ -conditional full-information constant Merton rule is

$$\pi^*(\theta) = \frac{\theta}{\gamma\sigma^2}. \quad (93)$$

Averaging this infeasible rule gives $\mathbb{E}[\pi^*(\theta)] = m/(\gamma\sigma^2)$. By contrast, the deployable θ -blind ex-ante optimizer within the constant-fraction class is

$$\pi_q^{\text{const}}(\tau) = \frac{m}{\gamma\sigma^2 + (\gamma-1)\tau p}, \quad (\gamma > 1), \quad (94)$$

which exhibits shrinkage due to estimation uncertainty ($p > 0$) and depends on the horizon τ . Thus $\mathbb{E}[\pi^*(\theta)] \neq \pi_q^{\text{const}}(\tau)$ whenever $p > 0$.

B.7 Implication for baselines in this paper

The discussion above motivates our baseline choices in the main text:

- We validate on controlled drift/premium benchmarks where closed-form *decision-time* Gaussian targets are available and match the fixed- q deployability restriction.
- For learning-based comparisons, we emphasize simulation-only direct policy search baselines (e.g., PPO) that operate under the same observation restriction (no access to θ ; θ sampled only inside the simulator), rather than value-function PDE/BSDE solvers whose natural DP target is belief-augmented.

C Proof of Theorem 2

Theorem 2 extends the BPTT–PMP (equivalently, BPTT–BSDE) correspondence established for deterministic-parameter models in our prior work on PG–DPO (see the main BPTT–BSDE correspondence result and proof in Huh et al. (2025a)). Here the only substantive change is that the market coefficients are indexed by a random but *frozen* parameter $\theta \sim q$, and we need convergence statements that hold *conditionally on θ* and *uniformly over θ* in compact subsets of Θ . (*This appendix replaces the current Appendix C in the draft.*)

Important remark (what this proof does *not* use). This proof concerns the θ -conditional Pontryagin adjoint/costate for the fixed- θ control problem induced by (45)–(46). It does *not* use the θ -blind q -aggregated stationarity condition (Theorem 1 in Section 3.2). Those constructions affect only stage 2 projection targets and are irrelevant to the BPTT–PMP convergence itself.

Notation, filtration, and the pathwise-vs-adapted issue. Fix $\theta \in \Theta$. We work conditionally on this θ and consider the augmented (simulator) filtration

$$\mathbb{G}^\theta := (G_t^\theta)_{t \in [0, T]}, \quad G_t^\theta := \sigma(\theta, \{W_s, W_s^Y : 0 \leq s \leq t\}) \text{ (with the usual augmentation).}$$

All conditional expectations and L^2 projections below are taken with respect to $G_{t_k}^\theta$.

Key point. The raw BPTT “adjoints” are *pathwise derivatives* of the terminal utility along the full discrete computation graph. Hence, for $k < N$, they are typically G_T^θ -measurable and need *not* be $G_{t_k}^\theta$ -measurable (they can depend on future increments). In contrast, the stochastic maximum principle (SMP/PMP) costate is \mathbb{G}^θ -adapted. Therefore, the correspondence is formulated *after* a standard one-step conditional L^2 projection (equivalently, a discrete-time BSDE representation), which turns pathwise objects into adapted discrete adjoints.

Let $\Delta t > 0$, $t_k := k\Delta t$, $k = 0, \dots, N$, $N\Delta t = T$. For readability we suppress the policy parameters φ and write $\pi_k := \pi_\varphi(t_k, X_k^\theta, Y_k^\theta)$, where π_φ is θ -blind but evaluated along the θ -conditional trajectory.

Step 1: Conditioning on θ and uniformity of bounds. Fix a compact set $K \subset \Theta$. Assume the coefficients in (45)–(46) satisfy the usual Lipschitz and linear-growth conditions *uniformly over $\theta \in K$* , and that the block covariance structure of (W, W^Y) (including instantaneous correlation) is uniformly nondegenerate on K . Assume also the regularity/integrability needed for the θ -conditional SMP (including the blocks relevant for the portfolio Hamiltonian gradient) to be well posed. Then, for each fixed $\theta \in K$, the controlled SDE system is well posed and admits uniform-in-time L^2 moment bounds. Moreover, the Euler–Maruyama scheme enjoys the standard strong error bound

$$\sup_{t \in [0, T]} \mathbb{E} \left[\left\| (X_t^{\pi, \theta}, Y_t^\theta) - (X_t^{\Delta t, \theta}, Y_t^{\Delta t, \theta}) \right\|^2 \right]^{1/2} \leq C_K \Delta t^{1/2},$$

with a constant C_K that can be chosen independently of $\theta \in K$. These are exactly the deterministic assumptions used in Huh et al. (2025a), now stated uniformly on K .

Step 2: Discrete forward scheme and BPTT pathwise adjoints (fixed θ). Under fixed θ , consider the Euler scheme on the grid (t_k) :

$$\begin{aligned} Y_{k+1}^\theta &= Y_k^\theta + a(Y_k^\theta, \theta) \Delta t + \beta(Y_k^\theta, \theta) \Delta W_k^Y, \\ X_{k+1}^\theta &= X_k^\theta + X_k^\theta \left(r + \pi_k^\top b(Y_k^\theta, \theta) \right) \Delta t + X_k^\theta \pi_k^\top \sigma(Y_k^\theta, \theta) \Delta W_k, \end{aligned}$$

with terminal reward $U(X_N^\theta)$. Define the discrete *pathwise* wealth costate

$$p_k^{\text{pw}, \theta} := \frac{\partial}{\partial X_k^\theta} U(X_N^\theta), \quad k = 0, \dots, N,$$

and the additional pathwise blocks

$$p_{x,k}^{\text{pw},\theta} := \frac{\partial p_k^{\text{pw},\theta}}{\partial X_k^\theta}, \quad p_{y,k}^{\text{pw},\theta} := \frac{\partial p_k^{\text{pw},\theta}}{\partial Y_k^\theta}.$$

Automatic differentiation/BPTT computes $\{(p_k^{\text{pw},\theta}, p_{x,k}^{\text{pw},\theta}, p_{y,k}^{\text{pw},\theta})\}_{k=0}^N$ via the backward chain rule along the discrete forward graph. The one-step algebraic form of the backward recursion coincides with the deterministic-parameter analysis in Huh et al. (2025a), with the replacements

$$\mu \mapsto b(\cdot, \theta), \quad \sigma \mapsto \sigma(\cdot, \theta),$$

and with the factor block handled exactly as in the wealth-factor extension therein. All one-step remainder terms are controlled by standard Taylor/Euler estimates with constants uniform in $\theta \in K$.

Step 3: Conditional L^2 projection \Rightarrow adapted discrete BSDE variables (fixed θ). Fix $\theta \in K$. Let $\Delta W_k := W_{t_{k+1}} - W_{t_k}$ and $\Delta W_k^Y := W_{t_{k+1}}^Y - W_{t_k}^Y$. Uniform nondegeneracy of the block covariance of $(\Delta W_k, \Delta W_k^Y)$ implies that the conditional L^2 -projection onto $\text{span}\{1, \Delta W_k, \Delta W_k^Y\}$ is well defined (and yields unique coefficients).

(a) *One-step projection (defining the discrete martingale coefficients).* Define $(z_k^\theta, \tilde{z}_k^\theta)$ by the conditional orthogonality relations (equivalently, the L^2 -projection) such that

$$p_{k+1}^{\text{pw},\theta} = \mathbb{E}\left[p_{k+1}^{\text{pw},\theta} \mid G_{t_k}^\theta\right] + z_k^\theta \Delta W_k + \tilde{z}_k^\theta \Delta W_k^Y + \varepsilon_{k+1}^\theta,$$

where ε_{k+1}^θ is orthogonal (in conditional L^2) to $\text{span}\{1, \Delta W_k, \Delta W_k^Y\}$ given $G_{t_k}^\theta$.

(b) *Adapted discrete adjoints (the objects compared to PMP).* Define the adapted discrete-time costates by conditional expectation:

$$p_k^{\Delta t,\theta} := \mathbb{E}\left[p_k^{\text{pw},\theta} \mid G_{t_k}^\theta\right], \quad p_{x,k}^{\Delta t,\theta} := \mathbb{E}\left[p_{x,k}^{\text{pw},\theta} \mid G_{t_k}^\theta\right], \quad p_{y,k}^{\Delta t,\theta} := \mathbb{E}\left[p_{y,k}^{\text{pw},\theta} \mid G_{t_k}^\theta\right].$$

These are $G_{t_k}^\theta$ -measurable and are the discrete-time counterparts of the θ -conditional Pontryagin objects.

(c) *Discrete BSDE form and identification of the driver.* Substituting the projection in (a) into the one-step BPTT recursion from Step 2 and then taking conditional expectations with respect to $G_{t_k}^\theta$ yields a canonical discrete-time BSDE representation for the adapted triple $(p_k^{\Delta t,\theta}, z_k^\theta, \tilde{z}_k^\theta)$. The resulting drift coincides with the Euler discretization of the θ -conditional adjoint BSDE associated with (45)–(46) under the fixed policy π_φ , up to standard one-step remainder terms of higher order in Δt . The same argument applies to the blocks $(p_{x,k}^{\Delta t,\theta}, p_{y,k}^{\Delta t,\theta})$: they satisfy linearized discrete backward recursions (obtained by differentiating the discrete adjoint equations) and hence admit analogous discrete-BSDE representations with coefficients uniformly controlled on K . All estimates and remainder controls are identical to Huh et al. (2025a) once we condition on θ , and the constants can be chosen uniformly on K by the uniform-in- θ assumptions from Step 1.

Step 4: Passage to continuous time and convergence to the θ -conditional PMP costate. For each fixed $\theta \in K$, the forward SDE and the θ -conditional adjoint BSDE form a standard FBSDE with coefficients parametrized by θ . Let $(p_t^\theta, p_{x,t}^\theta, p_{y,t}^\theta)$ denote the continuous-time θ -conditional Pontryagin objects under π_φ , with terminal condition $p_T^\theta = U'(X_T^{\pi,\theta})$.

Define the piecewise-constant interpolations of the *adapted* discrete variables:

$$p_t^{\Delta t,\theta} := p_k^{\Delta t,\theta}, \quad p_{x,t}^{\Delta t,\theta} := p_{x,k}^{\Delta t,\theta}, \quad p_{y,t}^{\Delta t,\theta} := p_{y,k}^{\Delta t,\theta}, \quad t \in [t_k, t_{k+1}).$$

Then, by the same stability and convergence arguments as in Huh et al. (2025a) (Euler convergence for the forward equation plus convergence of the discrete-BSDE scheme for the backward equation), we obtain, for each fixed $\theta \in K$,

$$\sup_{t \in [0, T]} \mathbb{E} [|p_t^{\Delta t, \theta} - p_t^\theta|^2] \rightarrow 0, \quad \sup_{t \in [0, T]} \mathbb{E} [\|p_{x,t}^{\Delta t, \theta} - p_{x,t}^\theta\|^2] \rightarrow 0, \quad \sup_{t \in [0, T]} \mathbb{E} [\|p_{y,t}^{\Delta t, \theta} - p_{y,t}^\theta\|^2] \rightarrow 0,$$

as $\Delta t \rightarrow 0$. Because all Lipschitz, growth, ellipticity, and block-covariance constants were assumed uniform on K , the constants in these convergence bounds can be chosen independently of $\theta \in K$. This yields the claimed BPTT–PMP correspondence conditionally on θ and uniformly over θ in compact subsets of Θ , completing the proof. \square

D Auxiliary results for Theorem 3

D.1 Stability of the projection map $(A, G) \mapsto -A^{-1}G$

Proposition 1 (Stability of the projection map $(A, G) \mapsto -A^{-1}G$). *Let D be a measurable domain and let μ be a reference measure on D . Let $A, \tilde{A} : D \rightarrow \mathbb{R}^{d \times d}$ and $G, \tilde{G} : D \rightarrow \mathbb{R}^d$ be measurable. Assume:*

- (i) $A(z)$ is invertible for μ -a.e. $z \in D$ and $\|A^{-1}\|_{L^\infty(D)} \leq \kappa$ for some $\kappa > 0$;
- (ii) $\|G\|_{L^\infty(D)} \leq M$ for some $M > 0$;
- (iii) $\|\tilde{A} - A\|_{L^\infty(D)} \leq (2\kappa)^{-1}$.

Define $\pi := -A^{-1}G$ and $\tilde{\pi} := -\tilde{A}^{-1}\tilde{G}$. Then $\tilde{A}(z)$ is invertible for μ -a.e. $z \in D$ with $\|\tilde{A}^{-1}\|_{L^\infty(D)} \leq 2\kappa$, and

$$\|\tilde{\pi} - \pi\|_{L^2(\mu)} \leq 2\kappa \|\tilde{G} - G\|_{L^2(\mu)} + 2\kappa^2 (M + \|\tilde{G}\|_{L^\infty(D)}) \|\tilde{A} - A\|_{L^2(\mu)}. \quad (95)$$

Proof. Throughout, $\|\cdot\|$ denotes the operator norm induced by the Euclidean norm.

Step 1: invertibility and uniform bound for \tilde{A}^{-1} . For μ -a.e. z , write

$$\tilde{A}(z) = A(z) \left(I + A(z)^{-1}(\tilde{A}(z) - A(z)) \right).$$

By (i) and (iii),

$$\|A^{-1}(z)(\tilde{A}(z) - A(z))\| \leq \|A^{-1}\|_{L^\infty(D)} \|\tilde{A} - A\|_{L^\infty(D)} \leq \kappa \cdot (2\kappa)^{-1} = \frac{1}{2}.$$

Hence $I + A^{-1}(\tilde{A} - A)$ is invertible and $\|(I + A^{-1}(\tilde{A} - A))^{-1}\| \leq (1 - \frac{1}{2})^{-1} = 2$. Therefore $\tilde{A}(z)$ is invertible and

$$\|\tilde{A}^{-1}(z)\| = \|(I + A^{-1}(\tilde{A} - A))^{-1}A^{-1}(z)\| \leq 2\|A^{-1}\|_{L^\infty(D)} \leq 2\kappa,$$

so $\|\tilde{A}^{-1}\|_{L^\infty(D)} \leq 2\kappa$.

Step 2: difference of inverses. Using the identity $\tilde{A}^{-1} - A^{-1} = \tilde{A}^{-1}(A - \tilde{A})A^{-1}$ and Hölder ($L^\infty \times L^2 \times L^\infty \rightarrow L^2$),

$$\|\tilde{A}^{-1} - A^{-1}\|_{L^2(\mu)} \leq \|\tilde{A}^{-1}\|_{L^\infty(D)} \|\tilde{A} - A\|_{L^2(\mu)} \|A^{-1}\|_{L^\infty(D)} \leq 2\kappa^2 \|\tilde{A} - A\|_{L^2(\mu)}.$$

Step 3: control error bound. Since $\pi = -A^{-1}G$ and $\tilde{\pi} = -\tilde{A}^{-1}\tilde{G}$,

$$\tilde{\pi} - \pi = -\tilde{A}^{-1}(\tilde{G} - G) - (\tilde{A}^{-1} - A^{-1})G.$$

Taking $L^2(\mu)$ norms and applying Hölder ($L^\infty \times L^2 \rightarrow L^2$) yields

$$\|\tilde{\pi} - \pi\|_{L^2(\mu)} \leq \|\tilde{A}^{-1}\|_{L^\infty(D)} \|\tilde{G} - G\|_{L^2(\mu)} + \|\tilde{A}^{-1} - A^{-1}\|_{L^2(\mu)} \|G\|_{L^\infty(D)}.$$

Using Step 1, Step 2, and (ii),

$$\|\tilde{\pi} - \pi\|_{L^2(\mu)} \leq 2\kappa \|\tilde{G} - G\|_{L^2(\mu)} + 2\kappa^2 M \|\tilde{A} - A\|_{L^2(\mu)} \leq 2\kappa \|\tilde{G} - G\|_{L^2(\mu)} + 2\kappa^2 (M + \|\tilde{G}\|_{L^\infty(D)}) \|\tilde{A} - A\|_{L^2(\mu)},$$

which is (95). \square

D.2 Slab-wise small-gain for the q -aggregated projection inputs

Time-slab decomposition. Assume the working domain carries a time coordinate and, for concreteness, $D \subset [0, T] \times S$ and $\mu(dt, d\xi) = dt \otimes \nu(d\xi)$ for some reference measure ν on S . Fix a partition $0 = t_0 < t_1 < \dots < t_K = T$ with slab lengths $\tau_k := t_k - t_{k-1}$ and define

$$D_k := D \cap ([t_{k-1}, t_k] \times S), \quad \mu_k := \mu|_{D_k}, \quad \|f\|_k := \|f\|_{L^2(\mu_k)}.$$

Then $\|f\|_{L^2(\mu)}^2 = \sum_{k=1}^K \|f\|_k^2$.

Proposition 2 (Short-time (slab) Lipschitz gain). *Let U be a neighborhood of a locally optimal deployable θ -blind policy π_{blind}^* in $L^2(\mu)$ such that for all $\pi \in U$,*

$$\|A_\pi^{-1}\|_{L^\infty(D)} \leq \kappa, \quad \|G_\pi^{\text{mix}}\|_{L^\infty(D)} \leq M_G$$

for some constants $\kappa, M_G > 0$. Assume that on each slab D_k the q -aggregated projection inputs satisfy

$$\|A_{\pi_1} - A_{\pi_2}\|_k \leq \bar{L}_A \tau_k^{1/2} \|\pi_1 - \pi_2\|_k, \quad \|G_{\pi_1}^{\text{mix}} - G_{\pi_2}^{\text{mix}}\|_k \leq \bar{L}_G \tau_k^{1/2} \|\pi_1 - \pi_2\|_k, \quad (96)$$

for all $\pi_1, \pi_2 \in U$, with constants $\bar{L}_A, \bar{L}_G > 0$ depending only on band data. Define the (population) projection map $T(\pi) := -A_\pi^{-1} G_\pi^{\text{mix}}$ and

$$\rho(\tau) := \left(\kappa \bar{L}_G + \kappa^2 M_G \bar{L}_A \right) \tau^{1/2}.$$

Then for each slab D_k and all $\pi_1, \pi_2 \in U$,

$$\|T(\pi_1) - T(\pi_2)\|_k \leq \rho(\tau_k) \|\pi_1 - \pi_2\|_k.$$

In particular, if the partition is chosen so that

$$\rho^* := \max_{1 \leq k \leq K} \rho(\tau_k) < 1,$$

then T is a strict contraction on every slab with constant at most ρ^* .

Proof. Fix k and $\pi_1, \pi_2 \in U$. Set $A_i := A_{\pi_i}$ and $G_i := G_{\pi_i}^{\text{mix}}$. Then

$$T(\pi_1) - T(\pi_2) = -A_1^{-1}(G_1 - G_2) - (A_1^{-1} - A_2^{-1})G_2, \quad A_1^{-1} - A_2^{-1} = A_1^{-1}(A_2 - A_1)A_2^{-1}.$$

Using Hölder ($L^\infty \times L^2 \rightarrow L^2$) on D_k together with $\|A_i^{-1}\|_{L^\infty(D)} \leq \kappa$ and $\|G_2\|_{L^\infty(D)} \leq M_G$ yields

$$\|T(\pi_1) - T(\pi_2)\|_k \leq \kappa \|G_1 - G_2\|_k + \kappa^2 M_G \|A_1 - A_2\|_k.$$

Applying (96) gives the claim with $\rho(\tau_k)$. □

Remark 3 (Where the $\tau^{1/2}$ gain comes from; relation to [huh2025a](#)). *The short-time factor $\tau^{1/2}$ in (96) is the same parabolic smoothing mechanism used in our earlier slab-wise PGDPO analysis:*

- One represents the relevant value-gap / adjoint differences on a short slab via a Duhamel (semigroup) formula, differentiates in space, and applies Young-type convolution bounds.
- In mixed norms, the gradient smoothing bound contributes a factor $\tau^{1/2-1/q}$ and the trivial embedding $L_t^\infty \hookrightarrow L_t^q$ contributes $\tau^{1/q}$, yielding net $\tau^{1/2}$.

A full PDE derivation of this short-time contraction philosophy is given in [Huh et al. \(2025a, Appendix B\)](#); see also the companion supplementary note to [Huh et al. \(2025a\)](#) (“On Proof of Theorem 4 (Policy Gap Bound)”) for a step-by-step slab contraction argument in a closely related setting. In the present paper the same smoothing principle is applied not to the costate update map directly, but to the induced q -aggregated projection inputs $(A_\pi, G_\pi^{\text{mix}})$.

D.3 Proof of Theorem 3

Proof of Theorem 3. We keep the notation of the main text. Let π^{warm} be the warm-up (deployable, θ -blind) policy and define the population q -aggregated projection inputs $(A_{\text{warm}}, G_{\text{warm}})$ by

$$A_{\text{warm}} := A_{\pi^{\text{warm}}}, \quad G_{\text{warm}} := G_{\pi^{\text{warm}}}^{\text{mix}}.$$

Define the *population projected* policy

$$\pi^{\text{proj}} := T(\pi^{\text{warm}}) = -A_{\text{warm}}^{-1}G_{\text{warm}}.$$

Let \hat{A} and \hat{G} be the stage-2 (BPTT/Monte Carlo) estimators of A_{warm} and G_{warm} used to form the deployable stage-2 control

$$\hat{\pi}_{\text{agg,mix}} := -\hat{A}^{-1}\hat{G}.$$

Let π_{blind}^* denote a locally optimal interior deployable θ -blind policy, so in particular it satisfies the fixed-point (stationarity) identity

$$\pi_{\text{blind}}^* = T(\pi_{\text{blind}}^*).$$

Step 1 (Estimator-to-population projection stability). Assume we are in the stable inversion regime (as enforced in practice by ridge/diagnostics) so that the hypotheses of Proposition 1 apply on D with $A = A_{\text{warm}}$ and $G = G_{\text{warm}}$. Then there exists a constant $C_2 > 0$ (depending only on the uniform inverse bound κ and uniform L^∞ bounds on the relevant G terms) such that

$$\|\hat{\pi}_{\text{agg,mix}} - \pi^{\text{proj}}\|_{L^2(\mu)} \leq C_2 \delta_{\text{BPTT}}, \quad (97)$$

where one convenient choice is

$$\delta_{\text{BPTT}} := \|\hat{A} - A_{\text{warm}}\|_{L^2(\mu)} + \|\hat{G} - G_{\text{warm}}\|_{L^2(\mu)}.$$

(Any equivalent control of the joint estimation error in (\hat{A}, \hat{G}) suffices.)

Step 2 (Slab-wise contraction for the population projection map). Assume $\pi^{\text{warm}}, \pi_{\text{blind}}^* \in U$ and let $\rho^* < 1$ be the slab contraction constant of Proposition 2. Since $\pi^{\text{proj}} = T(\pi^{\text{warm}})$ and $\pi_{\text{blind}}^* = T(\pi_{\text{blind}}^*)$, for each slab D_k we have

$$\|\pi^{\text{proj}} - \pi_{\text{blind}}^*\|_k = \|T(\pi^{\text{warm}}) - T(\pi_{\text{blind}}^*)\|_k \leq \rho(\tau_k) \|\pi^{\text{warm}} - \pi_{\text{blind}}^*\|_k \leq \rho^* \|\pi^{\text{warm}} - \pi_{\text{blind}}^*\|_k. \quad (98)$$

Step 3 (Residual identity and slab-wise warm-up deviation). Define the population mixed-moment aggregated stationarity residual of the warm-up policy

$$r_{\text{FOC,mix}}^{\text{warm}} := A_{\text{warm}}\pi^{\text{warm}} + G_{\text{warm}}, \quad \varepsilon_{\text{warm}}^{\text{mix}} := \|r_{\text{FOC,mix}}^{\text{warm}}\|_{L^2(\mu)}, \quad \varepsilon_{\text{warm},k}^{\text{mix}} := \|r_{\text{FOC,mix}}^{\text{warm}}\|_k.$$

By definition of π^{proj} ,

$$\pi^{\text{warm}} - \pi^{\text{proj}} = \pi^{\text{warm}} - (-A_{\text{warm}}^{-1}G_{\text{warm}}) = A_{\text{warm}}^{-1}(A_{\text{warm}}\pi^{\text{warm}} + G_{\text{warm}}) = A_{\text{warm}}^{-1}r_{\text{FOC,mix}}^{\text{warm}}.$$

Hence, on each slab,

$$\|\pi^{\text{warm}} - \pi^{\text{proj}}\|_k \leq \|A_{\text{warm}}^{-1}\|_{L^\infty(D)} \|r_{\text{FOC,mix}}^{\text{warm}}\|_k \leq \kappa \varepsilon_{\text{warm},k}^{\text{mix}}. \quad (99)$$

Step 4 (Slab-wise closure). Combine the triangle inequality with (98) and (99):

$$\|\pi^{\text{warm}} - \pi_{\text{blind}}^*\|_k \leq \|\pi^{\text{warm}} - \pi^{\text{proj}}\|_k + \|\pi^{\text{proj}} - \pi_{\text{blind}}^*\|_k \leq \kappa \varepsilon_{\text{warm},k}^{\text{mix}} + \rho^* \|\pi^{\text{warm}} - \pi_{\text{blind}}^*\|_k.$$

Since $\rho^* < 1$, we can close slab-wise:

$$\|\pi^{\text{warm}} - \pi_{\text{blind}}^*\|_k \leq \frac{\kappa}{1 - \rho^*} \varepsilon_{\text{warm},k}^{\text{mix}}. \quad (100)$$

Plugging (100) into (98) yields

$$\|\pi^{\text{proj}} - \pi_{\text{blind}}^*\|_k \leq \frac{\rho^* \kappa}{1 - \rho^*} \varepsilon_{\text{warm},k}^{\text{mix}}. \quad (101)$$

Step 5 (Global bound and completion). Sum over slabs using $\|f\|_{L^2(\mu)}^2 = \sum_k \|f\|_k^2$:

$$\|\pi^{\text{proj}} - \pi_{\text{blind}}^*\|_{L^2(\mu)} \leq \frac{\rho^* \kappa}{1 - \rho^*} \varepsilon_{\text{warm}}^{\text{mix}}.$$

Finally, combine with (97) and the triangle inequality:

$$\|\widehat{\pi}_{\text{agg},\text{mix}} - \pi_{\text{blind}}^*\|_{L^2(\mu)} \leq \|\widehat{\pi}_{\text{agg},\text{mix}} - \pi^{\text{proj}}\|_{L^2(\mu)} + \|\pi^{\text{proj}} - \pi_{\text{blind}}^*\|_{L^2(\mu)} \leq C_2 \delta_{\text{BPTT}} + \frac{\rho^* \kappa}{1 - \rho^*} \varepsilon_{\text{warm}}^{\text{mix}},$$

which is the claimed slab-wise residual-based θ -blind policy-gap bound. \square

E Implementation details for Section 3

This appendix provides reproducible step-by-step templates for the methods in Section 3. The high-level pipeline is summarized in Figure 4. For compactness we present one template per subsection of Section 3.

E.1 Stage 1 (PG–DPO) template for Section 3.1

Stage 1 performs stochastic gradient ascent on the fixed- q ex-ante objective (48), with latent $\theta \sim q$ sampled inside the simulator while the policy remains θ -blind.

Inputs. Policy parameters φ ; sampler ν over initial states; prior q ; time grid $(N, \Delta t)$; batch size M ; optimizer and step size α .

Template (one training iteration).

1. **Sample initial states.** Draw a mini-batch $\{z_0^{(i)} = (t_0^{(i)}, x_0^{(i)}, y_0^{(i)})\}_{i=1}^M \sim \nu$.
2. **Sample latent environment parameter.** Sample $\theta \sim q$ *inside the simulator* (unseen by π_φ). (Variant: sample $\theta^{(i)} \sim q$ independently per episode; both are unbiased for $\nabla_\varphi J(\varphi)$.)
3. **Simulate Euler rollouts.** For each episode i , simulate the Euler scheme in (45)–(46) under the θ -blind policy π_φ and collect terminal utilities $\{U(X_T^{(i)})\}_{i=1}^M$.
4. **Backpropagation through time (BPTT).** Compute the Monte Carlo gradient estimator

$$\widehat{g} \leftarrow \frac{1}{M} \sum_{i=1}^M \nabla_\varphi U(X_T^{(i)}).$$

5. **Parameter update.** Update $\varphi \leftarrow \varphi + \alpha \cdot \text{OptimizerStep}(\widehat{g})$, consistent with (50).
6. **Checkpoint.** Periodically save a warm-up checkpoint φ^{warm} for stage 2 projection.

E.2 Stage 2 (P–PGDPO projection; mixed-moment q -aggregation) template for Section 3.2

Stage 2 is a post-processing map: given a warm-up θ -blind policy $\pi_{\varphi^{\text{warm}}}$, it estimates Pontryagin sensitivity objects by Monte Carlo and constructs a *deployable* projected control on a working-domain sample $z \sim \mu$.

The aggregation used here matches the mixed-moment q -aggregation in (57)–(58), yielding the projected control (59).

Inputs. Warm-up policy $\pi_{\varphi^{\text{warm}}}$; working-domain sampler μ on D ; budgets $(M_z, M_\theta, M_{\text{MC}})$.

Template (constructing projection targets on a batch of query states).

1. **Sample working-domain query states.** Draw $\{z_j = (t_j, x_j, y_j)\}_{j=1}^{M_z} \sim \mu$.
2. **For each query state z_j , sample latent parameters.** Sample $\{\theta_\ell\}_{\ell=1}^{M_\theta} \sim q$.
3. **For each frozen θ_ℓ , estimate costates at z_j .** For each $\ell = 1, \dots, M_\theta$:
 - (a) Simulate M_{MC} trajectories from z_j under $\pi_{\varphi^{\text{warm}}}$ with frozen θ_ℓ .
 - (b) Compute pathwise sensitivities by autodiff/BPTT and average as in (54) to obtain $\hat{p}_t^{\theta_\ell}(z_j), \hat{p}_{x,t}^{\theta_\ell}(z_j), \hat{p}_{y,t}^{\theta_\ell}(z_j)$.
 - (c) Form the θ -conditional inputs (cf. (55)–(56)):

$$\hat{A}_t^{\theta_\ell}(z_j) \leftarrow x_j \hat{p}_{x,t}^{\theta_\ell}(z_j) \Sigma(y_j, \theta_\ell), \quad \hat{G}_t^{\theta_\ell}(z_j) \leftarrow \hat{p}_t^{\theta_\ell}(z_j) b(y_j, \theta_\ell) + \Sigma_{SY}(y_j, \theta_\ell) \hat{p}_{y,t}^{\theta_\ell}(z_j).$$
4. **Aggregate across $\theta \sim q$ (mixed-moment).** Compute

$$\hat{A}_t(z_j) \leftarrow \frac{1}{M_\theta} \sum_{\ell=1}^{M_\theta} \hat{A}_t^{\theta_\ell}(z_j), \quad \hat{G}_t^{\text{mix}}(z_j) \leftarrow \frac{1}{M_\theta} \sum_{\ell=1}^{M_\theta} \hat{G}_t^{\theta_\ell}(z_j),$$
 consistent with (57)–(58).
5. **Solve the projection (mixed-moment aggregation).** Whenever $\hat{A}_t(z_j)$ is invertible and the solve is numerically stable, compute the deployable projected control

$$\hat{\pi}^{\text{agg,mix}}(z_j) \leftarrow -(\hat{A}_t(z_j))^{-1} \hat{G}_t^{\text{mix}}(z_j),$$
 which matches (59).

E.3 Coupling I: residual/control-variate projection (Section F.1)

This subsection records a variance-reduced implementation of the stage 2 map using the residual identity (104). The residual form is applied around the warm-up policy and uses the mixed-moment aggregated inputs $(\hat{A}_t, \hat{G}_t^{\text{mix}})$.

Inputs. Warm-up policy $\pi_{\varphi^{\text{warm}}}$; query state(s) $z = (t, x, y) \sim \mu$; and stage 2 projection ingredients $(\hat{A}_t(z), \hat{G}_t^{\text{mix}}(z))$ constructed as in Section E.2.

Template (statewise residual projection; mixed-moment aggregation).

1. **Evaluate warm-up control.** Compute $\pi_{\varphi^{\text{warm}}}(z)$.
2. **Form the aggregated residual.** Compute

$$\hat{r}_{\text{FOC}}(z) \leftarrow \hat{A}_t(z) \pi_{\varphi^{\text{warm}}}(z) + \hat{G}_t^{\text{mix}}(z).$$

3. **Apply the residual correction.** Compute

$$\hat{\pi}^{\text{agg,mix}}(z) \leftarrow \pi_{\varphi^{\text{warm}}}(z) - (\hat{A}_t(z))^{-1} \hat{r}_{\text{FOC}}(z).$$

E.4 Coupling II: interactive distillation (Section F.2)

This subsection records an implementation template for interactive distillation: the projected output from stage 2 is used as a teacher signal during stage 1 training via the mixed objective (106). The teacher is built from the mixed-moment projected rule (possibly evaluated in residual form for variance reduction).

Inputs. Student parameters φ ; teacher refresh interval K ; distillation schedule $\lambda(n)$; working-domain sampler μ .

Template (training loop with intermittent teacher refresh).

1. **Initialize.** Set $\varphi^- \leftarrow \varphi$ and initialize an empty teacher buffer $\mathcal{B} \leftarrow \emptyset$.
2. **Repeat for iterations** $n = 1, 2, \dots$:
 - (a) **Stage 1 update (PG–DPO step).** Perform one PG–DPO update step on $J(\varphi)$ as in Section E.1.
 - (b) **Teacher refresh (every K steps).** If $n \bmod K = 0$:
 - i. Set $\varphi^- \leftarrow \varphi$ (lagged copy).
 - ii. Sample working-domain states $\{z_j\}_{j=1}^{M_z} \sim \mu$.
 - iii. For each z_j , run stage 2 under π_{φ^-} (mixed-moment aggregation) to compute a projected teacher $\hat{\pi}_{\varphi^-}^{\text{agg,mix}}(z_j)$. (In practice we compute it in residual form around π_{φ^-} as in (105).)
 - iv. Optionally filter states using diagnostics (Section E.5) and update the buffer:

$$\mathcal{B} \leftarrow \{(z_j, \hat{\pi}_{\varphi^-}^{\text{agg,mix}}(z_j))\}_{j=1}^{M_z} \text{ (after filtering).}$$

- (c) **Distillation step (when enabled).** If $\lambda(n) > 0$ and $\mathcal{B} \neq \emptyset$:
 - i. Sample (z, π^{teach}) from \mathcal{B} .
 - ii. Apply a gradient step to minimize the proximity term $\|\pi_{\varphi}(z) - \text{stopgrad}(\pi^{\text{teach}})\|^2$ with coefficient $\lambda(n)$, consistent with (106).

E.5 Engineering notes and stabilizers

This subsection collects practical stabilizers that we found helpful for reliable training and projection in high dimensions.

- **Antithetic sampling for θ .** When q is symmetric (e.g. Gaussian in a latent normal parameterization), sample θ in antithetic pairs by drawing $z \sim \mathcal{N}(0, I)$ and using $(z, -z)$ to construct (θ^+, θ^-) . This reduces the variance of q -averaged quantities and typically improves the stability of stage 2 diagnostics on the working domain.
- **Blockwise Monte Carlo and robust aggregation.** To control rare-tail domination, split Monte Carlo replications into B blocks and compute blockwise averages of costate-driven ingredients (e.g. $\hat{A}_t^\theta(z)$ and $\hat{G}_t^\theta(z)$). Aggregate across blocks using a robust statistic such as the median or median-of-means, which makes the projection less sensitive to outlier trajectories.
- **Curvature/denominator stability checks.** Because the projection map $(A, G) \mapsto -A^{-1}G$ can be sensitive to near-singularity of A , monitor the conditioning of \hat{A}_t (or failure rates of the linear solve). When diagnostics indicate ill-conditioning, skip projection-guided updates at that state or increase Monte Carlo budgets locally.

- **Residual magnitude as a reliability diagnostic.** For the residual form, compute $\hat{r}_{\text{FOC}}(z) = \hat{A}_t(z)\pi_{\varphi^{\text{warm}}}(z) + \hat{G}_t^{\text{mix}}(z)$. Small $\|\hat{r}_{\text{FOC}}(z)\|$ indicates approximate satisfaction of the mixed-moment aggregated first-order condition at z and empirically correlates with more reliable teacher targets.
- **Diagnostics-based teacher selection on the working domain.** Rather than applying distillation on all sampled $\{z_j\} \sim \mu$, keep only states that pass a reliability predicate. In practice, filter using residual-magnitude thresholds together with stable linear-solve diagnostics to prevent a small subset of pathological states from contaminating the teacher buffer.
- **λ schedule and safeguards.** Use a warm-up period with $\lambda = 0$ (pure PG–DPO) and increase λ only after stage 2 diagnostics on the working domain are stable. To prevent the teacher term from dominating the ex–ante objective, cap the effective coefficient via

$$\lambda_{\text{eff}} := \min \left\{ \lambda, c \frac{|L_{\text{main}}|}{L_{\text{distill}} + \varepsilon} \right\},$$

with $c \in (0, 1)$ and $\varepsilon > 0$.

- **Initialization and scale control in high dimensions.** To avoid early-time numerical blow-ups (often through quadratic variation terms of the form $\pi^\top \Sigma \pi$), initialize the policy output near zero and/or scale the output by $d^{-1/2}$. As a last-resort safety net, a mild log-wealth clamp can prevent overflow, but it should be used conservatively and monitored, since frequent clamping may distort higher-order sensitivities.

F Coupling stage 1 and stage 2: residual projection and interactive distillation

We keep the ex–ante objective (48) and the θ -blind deployability constraint throughout. Stage 2 is *not* a separate optimization problem: it is a (warm-started) post-processing map that reuses the current stage 1 policy as a warm-up control, estimates the projection ingredients under this warm-up policy, and then applies the q -aggregated Pontryagin projection as a deterministic transformation of the policy. Concretely, stage 2 takes π^{warm} as input, runs BPTT/Monte Carlo under frozen $\theta \sim q$ to estimate the adjoint blocks required for the Hamiltonian gradient, aggregates them across θ , and outputs a single deployable θ -blind rule $\hat{\pi}^{\text{agg,mix}}$ (Section 3.2).

This appendix records two couplings between the two stages, each with a distinct role:

- **Residual (control-variate) projection.** We compute the *same* projected rule in a residual form around the warm-up policy. This is algebraically equivalent to the direct projection, but typically reduces Monte Carlo variance and improves numerical stability in high dimensions.
- **Interactive distillation (amortized projection).** We use the projected rule as a teacher signal at intermittent refresh times. Beyond accelerating/stabilizing training, distillation amortizes the cost of projection: stage 2 can be accurate but Monte-Carlo intensive, whereas a distilled student policy approximates the projected rule with a single forward pass at stage 1 inference cost.

F.1 Control-variate (residual) form of the projected rule

Recall the mixed-moment projected rule (59). In high dimensions, Monte Carlo noise in the projection inputs can be non-negligible, and solving a linear system with \hat{A}_t can amplify this

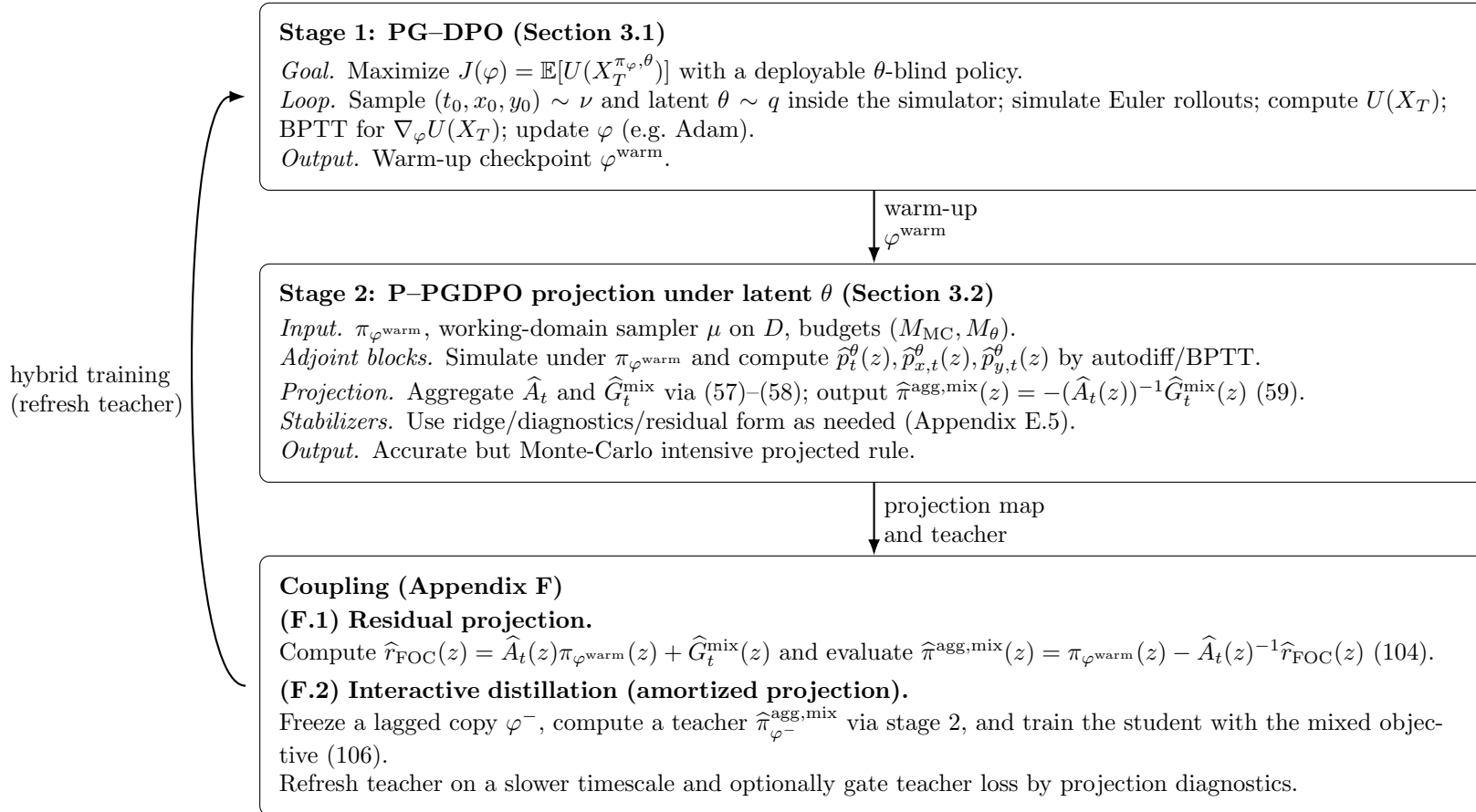


Figure 4: Pipeline of Section 3: stage 1 learning, stage 2 q -aggregated projection, and the coupling mechanisms in Appendix F. Distillation plays a dual role: it stabilizes training and amortizes the cost of projection by compressing projected controls into the policy network.

noise. A convenient stabilization is to compute the *same* projected rule in a residual (control-variate) form around the warm-up policy $\pi_{\varphi^{\text{warm}}}$.

Define the θ -conditional residual (under frozen- θ simulations)

$$\hat{r}_{\text{FOC}}^\theta(t, x, y) := \hat{A}_t^\theta(t, x, y) \pi_{\varphi^{\text{warm}}}(t, x, y) + \hat{G}_t^\theta(t, x, y), \quad (102)$$

and the aggregated residual (the quantity we actually solve against)

$$\hat{r}_{\text{FOC}}(t, x, y) := \hat{A}_t(t, x, y) \pi_{\varphi^{\text{warm}}}(t, x, y) + \hat{G}_t^{\text{mix}}(t, x, y). \quad (103)$$

Whenever $\hat{A}_t(t, x, y)$ is (numerically) invertible, the projected rule admits the identity

$$\hat{\pi}^{\text{agg,mix}}(t, x, y) = \pi_{\varphi^{\text{warm}}}(t, x, y) - \hat{A}_t(t, x, y)^{-1} \hat{r}_{\text{FOC}}(t, x, y), \quad (104)$$

which is an algebraic rewriting of (59) (hence it does not change the target).

Practical value (variance reduction and stability). When the warm-up policy is already close to a projected fixed point on the working domain, the residual \hat{r}_{FOC} tends to be small. Moreover, the ingredients entering $\hat{A}_t \pi_{\varphi^{\text{warm}}}$ and \hat{G}_t^{mix} are computed from the same Monte Carlo pool and often partially cancel, improving concentration of \hat{r}_{FOC} . In implementation, we combine (104) with the inversion stabilizers of Appendix E.5 (e.g. ridge regularization and diagnostic-based fallback to $\pi_{\varphi^{\text{warm}}}$ on unreliable states).

F.2 Interactive distillation: projection-guided training and amortized deployment

Let π_φ be the trainable stage 1 policy network. At intermittent refresh times, we freeze a lagged copy π_{φ^-} and run stage 2 under π_{φ^-} to construct a q -aggregated projected teacher. This coupling serves two purposes:

- **Training aid.** Projection-guided targets can stabilize and accelerate stage 1 optimization, especially once the warm-up policy enters a locally stable regime.
- **Amortization.** Stage 2 projection can be accurate but Monte-Carlo intensive; distillation compresses it into a single forward pass for deployment.

Teacher definition (computed by stage 2, treated as fixed). In residual form (104), the teacher is the θ -blind map

$$\hat{\pi}_{\varphi^-}^{\text{agg,mix}}(t, x, y) := \pi_{\varphi^-}(t, x, y) - (\hat{A}_t^{\varphi^-}(t, x, y))^{-1} \hat{r}_{\text{FOC}}^{\varphi^-}(t, x, y), \quad (105)$$

where $\hat{r}_{\text{FOC}}^{\varphi^-} := \hat{A}_t^{\varphi^-} \pi_{\varphi^-} + \hat{G}_t^{\text{mix}, \varphi^-}$ is computed using the mixed-moment q -aggregation under the lagged policy. In practice, the inversion in (105) is implemented with the same stabilizers as in Section 3.2 (ridge/diagnostics/residual form); for notational simplicity we keep the formal inverse.

Student objective (hybrid PG–DPO + distillation loss). We train π_φ by combining the original ex-ante objective with a proximity term to the teacher on the working domain:

$$\max_{\varphi} J(\varphi) - \lambda \mathbb{E}_{(t, x, y) \sim \mu} \left[\|\pi_\varphi(t, x, y) - \text{stopgrad}(\hat{\pi}_{\varphi^-}^{\text{agg,mix}}(t, x, y))\|^2 \right], \quad (106)$$

where μ is the working-domain sampling measure and $\lambda \geq 0$ controls the strength of projection guidance. The operator $\text{stopgrad}(\cdot)$ indicates that gradients are not propagated through stage 2: once computed from π_{φ^-} , the teacher is treated as fixed.

Refresh schedule, annealing, and diagnostic gating (implementation). In practice, φ^- and $\hat{\pi}_{\varphi^-}^{\text{agg,mix}}$ are refreshed on a slower timescale than the stage 1 gradient steps. A typical and robust configuration is:

- **Two-time-scale refresh.** Hold φ^- fixed for K_{refresh} stage 1 updates of φ under (106), then set $\varphi^- \leftarrow \varphi$ and recompute the teacher via stage 2.
- **Anneal λ .** Start with $\lambda = 0$ (pure PG–DPO) and increase λ only after basic projection checks on the working domain indicate that the stage 2 map is reliable. Concretely, we anneal λ toward a target value λ_{max} once the warm-up residual $\|\hat{r}_{\text{FOC,mix}}^{\text{warm}}\|_{L^2(\mu)}$ and curvature diagnostics remain stable over several refresh cycles.
- **Adaptive teacher selection (gating).** To avoid injecting noisy teacher targets early in training or on pathological regions of the domain, we optionally apply the teacher loss only on states where projection diagnostics certify reliability (e.g. bounded condition number of \hat{A}_t , eigenvalue/denominator lower bounds, and moderate residual magnitude), falling back to pure PG–DPO elsewhere.

Implementation details, including the precise diagnostics and stabilizers, are deferred to Appendix E.

Deployment. After training, the deployed controller is simply the student network π_φ , which approximates the stage 2 projected rule with a single forward pass, without repeatedly running BPTT/Monte Carlo projection at inference time.

G Stage 2 projection diagnostics

We report Stage 2 diagnostic statistics as a visual supplement to Section 4.2. Each figure summarizes the same tail-median protocol and layout; see captions for definitions and interpretation.

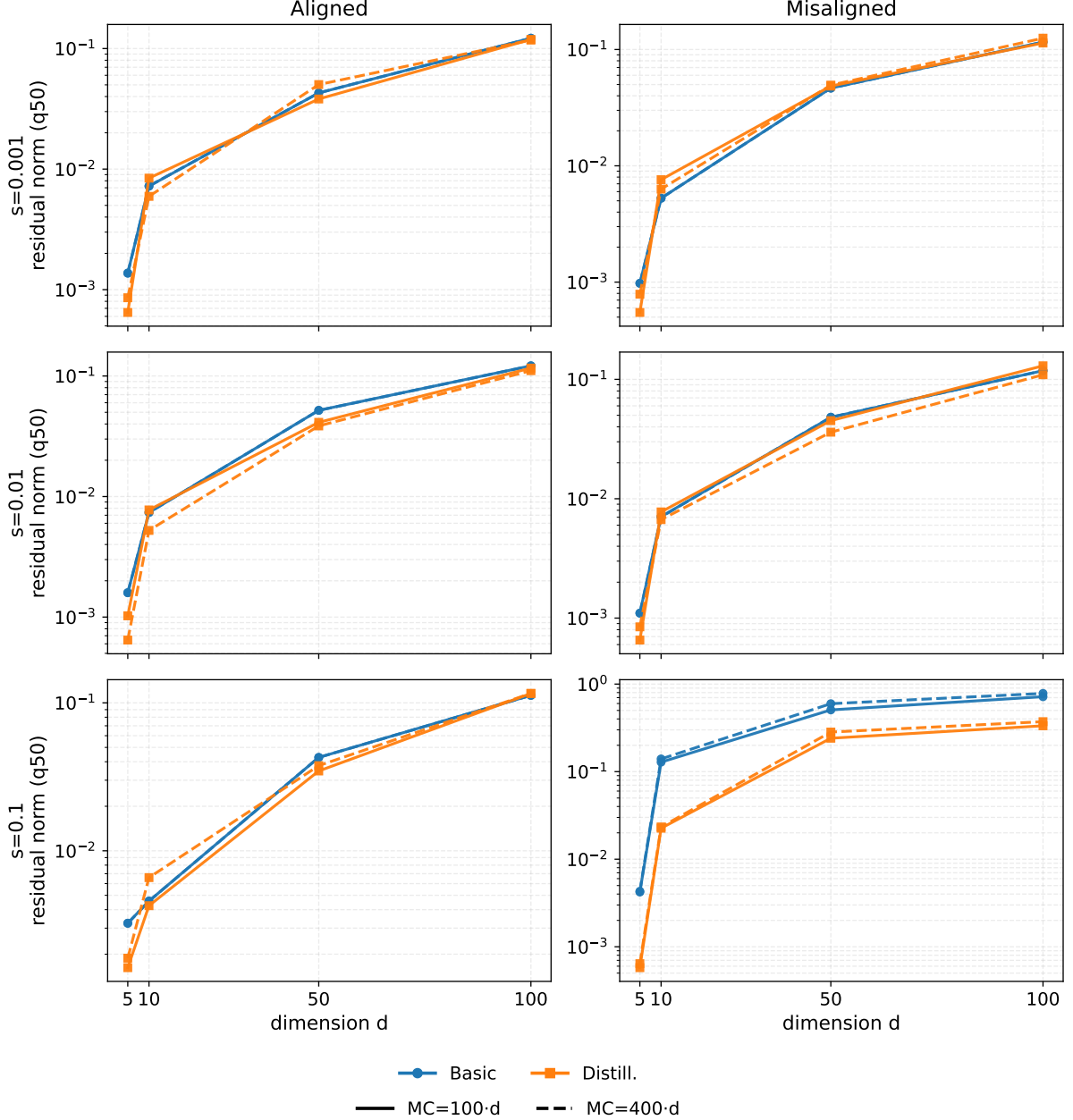


Figure 5: **Stage 2 stationarity residual (q50).** All panels report tail medians over epochs 9500–10000 (final six evaluation snapshots). Layout matches Figure 2: rows correspond to $s \in \{10^{-3}, 10^{-2}, 10^{-1}\}$ and columns correspond to aligned vs. misaligned uncertainty. Solid vs. dashed lines are MC base ($100 \cdot d$) vs. high ($400 \cdot d$). We plot the median (q50) of the estimated Hamiltonian first-order condition residual norm at the query states. Larger residual indicates the warm policy is farther from stationarity, implying a larger correction is required in the residual-form projection. Growth of this residual with d (especially under misalignment) supports the mechanism that projection becomes more sensitive in high dimension due to larger correction magnitudes and amplified mixed-moment noise.

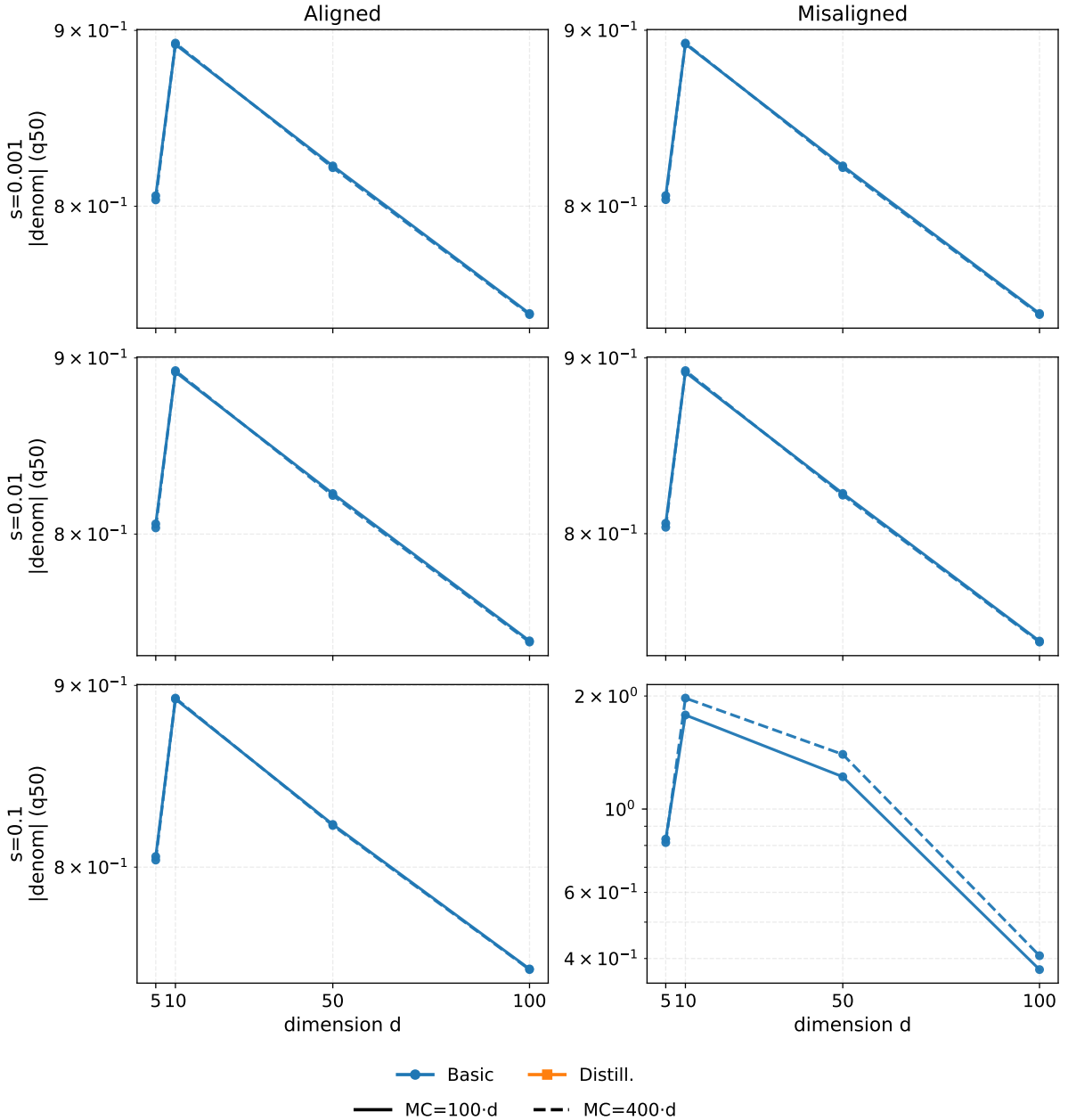


Figure 6: **Stage 2 denominator magnitude (q50).** All panels report tail medians over epochs 9500–10000 (final six evaluation snapshots). Layout matches Figure 2: rows correspond to $s \in \{10^{-3}, 10^{-2}, 10^{-1}\}$ and columns correspond to aligned vs. misaligned uncertainty. Solid vs. dashed lines are MC base ($100 \cdot d$) vs. high ($400 \cdot d$). We plot a typical (q50) magnitude of the projection denominator/curvature term used in the residual-form update. Values bounded away from zero indicate that projection is not operating in a near-singular regime at typical quantiles. This helps rule out “catastrophic inversion” as the primary driver of degradation; instead, residual growth and curvature mismatch (Fig. 7) provide a more consistent explanation in misaligned/high- d regimes.

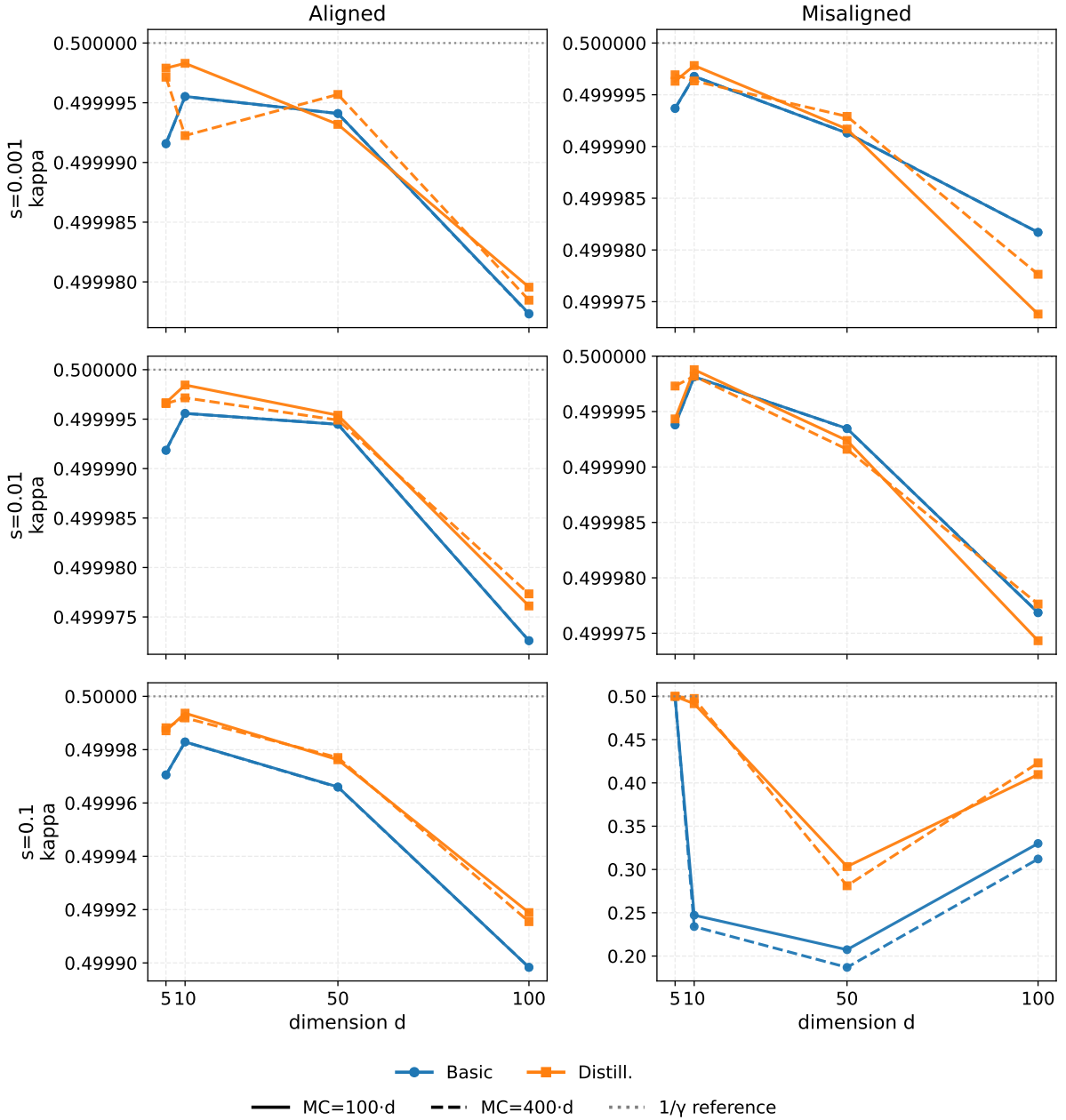


Figure 7: **Stage 2 curvature-consistency statistic κ .** All panels report tail medians over epochs 9500–10000 (final six evaluation snapshots). Layout matches Figure 2: rows correspond to $s \in \{10^{-3}, 10^{-2}, 10^{-1}\}$ and columns correspond to aligned vs. misaligned uncertainty. Solid vs. dashed lines are MC base ($100 \cdot d$) vs. high ($400 \cdot d$). We report the stabilized median-after-floor statistic κ and compare it to the nominal reference $1/\gamma$ (horizontal dotted line). For CRRA, costate ratios imply a characteristic curvature scale; sustained deviations of κ from $1/\gamma$ indicate costate inconsistency and/or bias in mixed-moment estimation, and are most visible in the hardest misaligned/high-uncertainty regime.

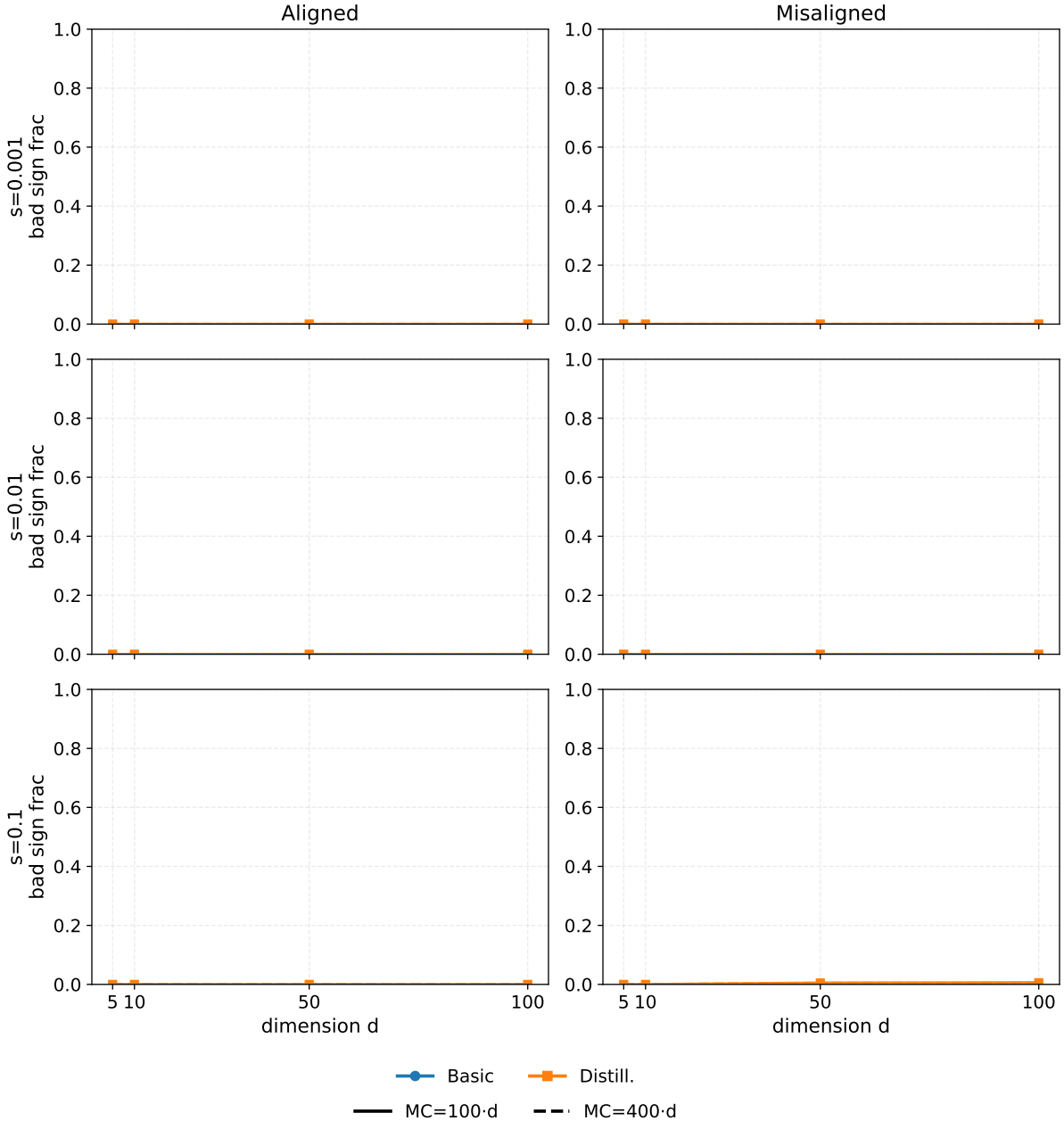


Figure 8: **Stage 2 bad-sign fraction.** All panels report tail medians over epochs 9500–10000 (final six evaluation snapshots). Layout matches Figure 2: rows correspond to $s \in \{10^{-3}, 10^{-2}, 10^{-1}\}$ and columns correspond to aligned vs. misaligned uncertainty. Solid vs. dashed lines are MC base ($100 \cdot d$) vs. high ($400 \cdot d$). We plot the fraction of samples in which the estimated curvature/denominator violates the expected sign condition (loss of local concavity on the sampled batch). Near-zero bad-sign fractions across most regimes suggest that the projection typically operates in a locally well-behaved region and that failures are not dominated by sign flips, supporting the main-text conclusion that misalignment primarily increases residual/costate mismatch rather than inducing widespread concavity violations.

H Supplementary decomposition diagnostics for Section 5

Tables 4–5 report Stage 2 decomposition diagnostics at $t = 0$.

s_0	Method	$d = 5$	10	50	100
Aligned P_0					
10^{-3}	Stage 1+Stage 2 (Basic)	7.17×10^{-6}	1.51×10^{-5}	1.60×10^{-5}	1.23×10^{-5}
	Stage 1+Stage 2 (Distill.)	5.20×10^{-6}	9.81×10^{-6}	1.64×10^{-5}	1.62×10^{-5}
10^{-2}	Stage 1+Stage 2 (Basic)	6.21×10^{-6}	1.38×10^{-5}	1.63×10^{-5}	1.42×10^{-5}
	Stage 1+Stage 2 (Distill.)	7.13×10^{-6}	7.13×10^{-6}	1.62×10^{-5}	1.76×10^{-5}
10^{-1}	Stage 1+Stage 2 (Basic)	8.18×10^{-6}	1.41×10^{-5}	3.82×10^{-5}	2.42×10^{-5}
	Stage 1+Stage 2 (Distill.)	6.72×10^{-6}	9.21×10^{-6}	3.67×10^{-5}	3.16×10^{-5}
Misaligned P_0					
10^{-3}	Stage 1+Stage 2 (Basic)	1.10×10^{-5}	1.41×10^{-5}	1.70×10^{-5}	1.18×10^{-5}
	Stage 1+Stage 2 (Distill.)	7.71×10^{-6}	5.94×10^{-6}	1.84×10^{-5}	1.62×10^{-5}
10^{-2}	Stage 1+Stage 2 (Basic)	7.90×10^{-6}	2.02×10^{-5}	1.46×10^{-5}	1.20×10^{-5}
	Stage 1+Stage 2 (Distill.)	6.00×10^{-6}	1.71×10^{-5}	2.21×10^{-5}	1.43×10^{-5}
10^{-1}	Stage 1+Stage 2 (Basic)	1.24×10^{-5}	1.93×10^{-4}	5.77×10^{-5}	3.14×10^{-5}
	Stage 1+Stage 2 (Distill.)	1.20×10^{-5}	1.90×10^{-4}	7.40×10^{-5}	2.47×10^{-5}

Table 4: Myopic-component RMSE at $t = 0$ (tail medians).

s_0	Method	$d = 5$	10	50	100
Aligned P_0					
10^{-3}	Stage 1+Stage 2 (Basic)	0.994	0.988	0.991	0.990
	Stage 1+Stage 2 (Distill.)	0.995	0.986	0.990	0.987
10^{-2}	Stage 1+Stage 2 (Basic)	0.993	0.989	0.992	0.988
	Stage 1+Stage 2 (Distill.)	0.992	0.994	0.990	0.987
10^{-1}	Stage 1+Stage 2 (Basic)	0.988	0.990	0.936	0.932
	Stage 1+Stage 2 (Distill.)	0.996	0.990	0.949	0.922
Misaligned P_0					
10^{-3}	Stage 1+Stage 2 (Basic)	0.988	0.988	0.993	0.990
	Stage 1+Stage 2 (Distill.)	0.994	0.995	0.990	0.987
10^{-2}	Stage 1+Stage 2 (Basic)	0.994	0.976	0.992	0.988
	Stage 1+Stage 2 (Distill.)	0.994	0.980	0.988	0.989
10^{-1}	Stage 1+Stage 2 (Basic)	0.990	0.005	0.668	0.851
	Stage 1+Stage 2 (Distill.)	0.992	-0.009	0.642	0.871

Table 5: Hedging-direction cosine similarity at $t = 0$ (tail medians). Higher is better; negative indicates direction reversal.